Automated Characterization of Drilling Fluid Properties

APPROVED BY

SUPERVISING COMMITTEE:

Eric van Oort, Supervisor

Ali Karimi

Automated Characterization of Drilling Fluid Properties

by

Gregory John Sullivan, B.S.

THESIS

Presented to the Faculty of the Graduate School of

The University of Texas at Austin

in Partial Fulfillment

of the Requirements

for the Degree of

MASTER OF SCIENCE IN ENGINEERING

THE UNIVERSITY OF TEXAS AT AUSTIN

December 2016

Acknowledgments

I wish to sincerely thank my advisor, Dr. Eric van Oort whose guidance and mentorship has greatly helped me in my development as an engineer. The opportunities he has exposed me to have proved extremely useful and will stay with me through my career.

I would additionally like to thank Dr. Ali Karimi for his assistance and mentorship through my research. Without his help, my research would have never reached the levels it did. I would like to thank Besmir Hoxha for his assistance as my lab supervisor; his patience allowed me to quickly integrate myself into my research. I would like to thank Walter Mayfield, Tesse Smitherman, the entire RAPID Consortium, and all of my fellow colleagues for their support, assistance, and guidance.

I would like to thank Tim Hooper, Gary Miscoe, Glen Baum, and Daryl Nygaard for their assistance.

Finally, I would like to thank my family and friends. It has been a wonderful journey, and I could not have achieved this without you.

Automated Characterization of Drilling Fluid Properties

Gregory John Sullivan, M.S.E.
The University of Texas at Austin, 2016

Supervisor: Eric van Oort

Accurate measurement of drilling fluid properties is essential in order to optimize wellbore construction, and in particular to properly manage hydraulics. It becomes even more crucial during deepwater drilling when a narrow mud window is present which may require the use of more advanced drilling technologies such as Managed Pressure Drilling (MPD) and Dual Gradient Drilling (DGD). Operating these technologies properly requires the use of sophisticated hydraulic models which require accurate rheological information as input. However, a full mud check with determination of all relevant rheological parameters is usually only carried out once per day, and augmented with one or two partial checks in the 24-hour period. Such intermittent and unreliable measurements are unfortunately not sufficient to provide the required inputs for 'real-time' hydraulic modeling and control. A more practical approach for a continuous, automated monitoring of the drilling fluid properties is therefore called for.

The method used here is based on the pipe viscometer approach rather than the traditional rotational viscometer method. In addition to the fluid rheology, important inputs for hydraulic models, such as mud density, transition to turbulent flow (critical Reynolds number), and real-time friction factor for non-Newtonian drilling and completion fluids are also obtained using the pipe viscometer. A prototype of this equipment was constructed, tested, and fully automated at The University of Texas at Austin.

The flow loop was tested with several weighted and unweighted mud systems. During the measurement process, the driving pump was ramped up and held intermittently at various flow rates to measure the laminar frictional pressure loss in the pipe section. The data thus obtained was analyzed by software that generated a flow curve and from it derived relevant mud rheological parameters using a suitable rheological model. It also proved possible to extend the test to the turbulent flow regime and obtain the 'true' friction factor in real-time for each particular fluid, rather than relying on a limited number of correlations that quite often exhibit inaccurate results, particularly for the Yield Power Law (YPL) fluids. Several successful tests with different mud systems indicate the reliability and robustness of the proposed technique.

Table of Contents

List of Tables

List of Figures

Chapter 1

Introduction

Accurate knowledge of drilling fluid properties and the associated hydraulics are critical to the drilling procedure. Standards for drilling fluid characterization, particularly those contained in API Standards 13B-1 & 2 (2003), are rightly held in high regard, as they have served the industry well for decades. However, many of the measurement test protocols are now rather antiquated and generally do not reflect current state-of-the-art tool and sensor design, data acquisition and analysis techniques, etc. (Karimi Vajargah and van Oort, 2015b). For instance, rotational type rheometers are still widely used in the oil and gas industry to determine and predict the flow character of drilling fluids.

Continuous monitoring of drilling fluid rheology will result in prevention and/or early detection of some major drilling problems such as those associated with drilling fluid contamination, wellbore cleaning problems, wellbore instability, etc. In addition, continuous monitoring will alleviate sensitivity to sampling issues that plague current measurement. Moreover, the rheology of a drilling fluid that is being circulated through a well may change due to several factors such as the application of shearing forces, variations in pressure and

temperature, introduction of drilling cuttings, contaminants, etc. Continuous monitoring allows for real-time evaluation and management of these changes.

With the recent introduction of advanced technologies such as Managed Pressure Drilling (MPD) and Dual Gradient Drilling (DGD), frequent and accurate measurement of drilling fluid characteristics are becoming even more important and necessary. Note that the sophisticated hydraulics models, which are used in MPD/DGD control operations, are only as good as their input parameters, and the parameters that matter the most are those associated with rheology, density, friction factor, and flow regime transition points (Karimi Vajargah et al., 2016).

The majority of problems encountered in drilling can be traced back to sub-optimal drilling fluid properties. Although the cost of the drilling fluid itself is relatively small in comparison to the overall cost of drilling, the costs due to problems encountered when using an improper drilling fluid can be extremely expensive (Mitchell et al., 2011).

Downhole fluid pressure must be accurately represented in order to avoid influxes and lost circulation events. Assuming that the fluid is incompressible, static pressure exerted by the fluid can be easily calculated by using the equation:

$$\Delta P_{static} = \rho g h \tag{1.1}$$

When the fluid is moving however, frictional pressure losses add to

the pressure seen downhole. This is taken into account using the equivalent circulating density (ECD) which is calculated by:

$$ECD = \frac{\Delta P_{static} + \Delta P_{fric,annular}}{gh} \tag{1.2}$$

In areas where the well is exposed to the formation, ECD must always be maintained within a given range known as the 'mud window'. The mud window is the range of ECD values that avoid drilling problems based upon downhole pressure. Downhole pressure measurement devices are not always available; therefore, the ECD value is often calculated using models. The parameters input into the model are often delivered as part of a 'mud check' routine.

Mud checks are usually conducted at atmospheric pressure using test protocols standardized by API 13 B-1 & 2 (2003). Measurements depend on the availability of the mud engineer and are only conducted a few times during a 24-hour period. Often, a full mud check with determination of all relevant rheological parameters is only carried out once a day, which is then augmented with one or two partial checks in the 24-hour period. Therefore, many critical downhole decisions made by operators are based on drilling fluid data that could be up to 24-hours old (Broussard, 2010). When applying a rotational rheometer at the rig site, quite often shear stress readings at only two shear rates (300 and 600 rpm) are used to characterize the fluid, which may result in oversimplified values for fluid rheological parameters and hence poor

hydraulic management. Accurate determination of rheological parameters is crucial during complex drilling operations, where a correct calculation of the frictional pressure losses and the associated ECD is vital.

To date, most attempts to automate drilling fluid rheological property measurement have merely tried to automate the conventional measurement devices, presumably out of habit and respect for the API standards (e.g., Stock et al., 2012; Hensley et al., 1985). A newer, automated version of the portable viscometer has been introduced (for instance, see Saasen et al., 2009). To the best of our knowledge, no method has yet been proposed for real-time determination of friction factor of non-Newtonian drilling fluids in the turbulent flow regime.

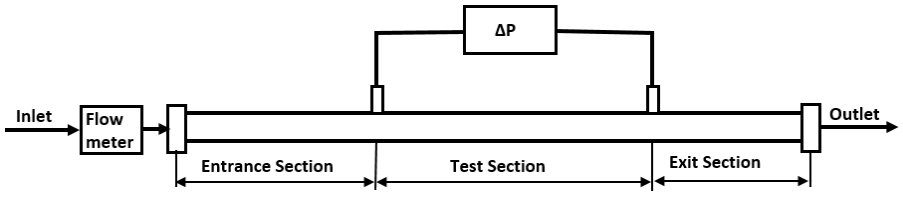

Figure 1.1: Pipe viscometer system schematic requiring a flow meter and a differential pressure sensor.

Due to its design, a pipe viscometer is inherently better suited for automation purposes than a rotational viscometer. A standard pipe viscometer system, shown in Figure 1.1 employs instrumentation for flow rate and pressure loss measurements. The pipe viscometer can be installed at several possible locations at the rig site, as shown in Figure 1.2. One simple example is to install the pipe viscometer right after the main mud pump and before the

standpipe. In this case, when the pump is staged either up or down, pressure loss can be measured at several flow rates, which then can be used to determine rheological properties. The advantage of this method is that measurements are done at elevated pressure when the fluid has been energized by the mud pumps. The downside of this method is that it jeopardizes the (high-) pressure integrity of the standpipe system. Additionally, in this case the test is limited because the drilling process will likely not reach as many steady state flow rates as desired for a full rheological model to be developed.

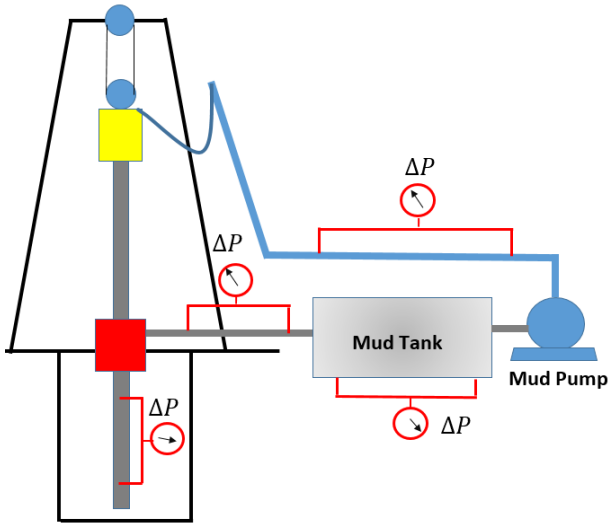

Figure 1.2: Potential locations to install a pipe viscometer in the field.

Another possibility is to install a sampling system (including a sampling port and tank) and pipe viscometer before the main pump, as shown in Figure 1.3, or simply alongside the array of mud pits on a drilling rig. The preferred location is after the mud pits, where drilling fluid has been processed and cleaned (by shale shakers, hydro-cyclones (desanders and desilters), degassers,

and centrifuges) such that the pipe viscometer lines will not become plugged with solids. This setup relies on a separate auxiliary pump that can be easily automated to apply a series of stepped flow rates, in order to measure the pressure loss at each flow rate and to calculate the rheological properties. Since such a set up does not rely on the main mud pumps, it can be used regardless of mud pump utilization or ongoing rig operations.

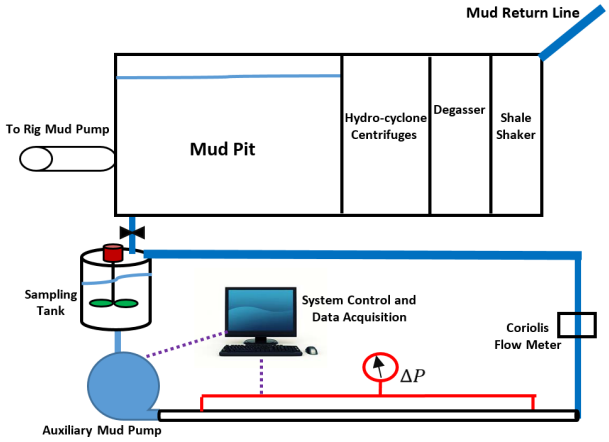

Figure 1.3: A pipe viscometer is installed alongside the mud pits (applicable to the field and also mud plants). An auxiliary pump and an accurate mass flow meter (e.g. Coriolis) are required for this set up.

In addition to rheology testing (done at laminar flow rates), tests were performed at higher flow rates to better characterize how the fluid behaved in transitional and turbulent flow regimes which often occur in drillpipe and drill collars. In such a case, we do not need to rely on friction factor equations to predict pressure drop values for non-Newtonian fluids.

A final set of tests were performed to show the effectiveness of friction reducers used to reduce drag in frac fluids. Many of the current products

used to reduce fluid friction are tested and developed within the confines of a lab at 'ideal conditions'. When salt, or other contaminants, are found in the fluid (as they are in real world applications) the effectiveness of these products is significantly reduced. Additionally, at high shear, many of these products permanently lose their friction reducing qualities after just a few minutes. Better understanding these complications could significantly save costs in pumping and improve overall frac jobs.

Chapter 2 presents a review of previous research efforts regarding pipe viscometry, transitional and turbulent flow of non-Newtonian fluids, and friction reducers used in the oil and gas industry.

Chapter 3 discusses the equipment and automation software required to analyze the results of the pipe viscometer. The setup of the in-lab pipe viscometer is presented and discussed. Recommendations for real world components are made when beneficial.

Chapter 4 is where results are presented and discussed. Results include laminar, transitional, and turbulent data for a variety of muds. Additionally, a section dedicated to friction factor reduction is included.

Chapter 5 concludes the thesis and provides suggestions for future work.

Chapter 2

Literature Review

2.1 Drilling Mud Rheology

Several types of viscometers are available to measure drilling fluid rheological properties. According to Ahmed and Miska (2009), pipe viscometers often show better reliability and accuracy than rotational viscometers. The idea of using a pipe viscometer to determine the fluid rheological properties is not new; for instance, Suzuki (1994) proposed an in-line viscometry method based on annulus liquid flow to measure non-Newtonian properties of food for quality and process control. However, there is no published record of this technique being applied on the rig site for real-time monitoring of drilling fluid properties. Karimi Vajargah and van Oort (2015a) used distributed downhole pressure data provided by wired drill pipe to obtain drilling fluid rheological parameters under downhole conditions, i.e. rheology at actual downhole pressures and temperatures. In many drilling operations, however, such pressure data may not be available. Therefore a similar, more cost effective concept is applied here to characterize rheological properties at surface.

There are many fluid flow models relevant to drilling operations. The most common flow profiles used in drilling fluid analysis are:

Newtonian:

$$\tau = K\gamma \tag{2.1}$$

Bingham Plastic:

$$\tau = \tau_y + K\gamma \tag{2.2}$$

Power Law:

$$\tau = K\gamma^m \tag{2.3}$$

and Yield Power Law (also known as Herschel Bulkley):

$$\tau = \tau_y + K\gamma^m \tag{2.4}$$

The Yield Power Law (YPL) model is often used in the field and most accurately portrays the fluid parameters for drilling muds. Because of this, the YPL model is used throughout this thesis. It is important to note that if the yield stress, τ_y, is equal to zero, the YPL model converts to the Power Law model. Additionally, if the consistency index, m, is equal to one, the model converts to the Bingham Plastic model.

To build this model, frictional pressure loss is recorded within the laminar flow regime. Typically, fluid rheological parameters are expressed as wall shear stress τ_w versus nominal Newtonian shear rate $8v/D$.

Shear stress at the wall (assuming no slip) is:

$$\tau_w = \frac{D}{4}\frac{dp}{dl} \tag{2.5}$$

Shear rate can be expressed as:

$$\gamma = -(\frac{dv}{dr}) \tag{2.6}$$

For a YPL fluid, the shear rate at the wall is given as (Ahmed and Miska, 2009):

$$\dot{\gamma}_w = (\frac{3N+1}{4N})\frac{8v}{D} \tag{2.7}$$

where:

$$N = \frac{d(ln\tau_w)}{d(ln\frac{8v}{D})} \tag{2.8}$$

The natural logarithm of shear stress versus the natural logarithm shear rate represents the flow curve. N, the generalized flow behavior index, is the derivative of the flow curve profile at any given location. A full derivation of Equation 2.7 can be seen in Appendix C.

Due to the precision required, determination of the N value is the most difficult parameter to obtain on a consistent and accurate level. Lazarus and Slatter (1988) show that while a curve fit through analytical data for N is attractive, obtaining reliable data from actual viscometry data is difficult. Finding the N value is the driving force behind high accuracy requirements for measuring devices.

2.2 Drilling Mud Transitional/Turbulent Flow

In order to establish the flow regime, the critical Reynolds number for transition from laminar to turbulent flow must be characterized (Ahmed and Miska, 2009). Although the critical Reynolds number of approximately 2100 (note that the Reynolds number is dimensionless) is extensively used for Newtonian fluids, some fluids (especially viscoelastic fluids) tend to delay and complicate this transition. For Yield Power Law fluids, we characterize the Reynolds number as:

$$Re_{YPL} = \frac{8\rho v^2}{\tau_y + K\gamma^m} \tag{2.9}$$

Friction factor is used to calculate the pressure loss in a pipe. Pressure loss and friction factor for a given fluid are related through the equation:

$$\frac{dp}{dl} = \frac{2f\rho v^2}{D} \tag{2.10}$$

The Fanning friction factor for laminar flow in circular tubes is:

$$f = \frac{16}{Re} \tag{2.11}$$

As shown by Dodge and Metzner (1959) the friction factor for a YPL fluid in turbulent flow can be estimated as:

$$\frac{1}{\sqrt{f}} = \frac{4}{m^{0.75}} log(Re \times f^{1-\frac{m}{2}}) - \frac{0.4}{m^{1.2}} \tag{2.12}$$

Chilton and Stainsby (1998) note that due to the complexity and diversity of non-Newtonian fluids, development of universal equations to predict

pressure loss have proceeded much more slowly than for Newtonian fluids. Although much work has been put into developing transitional and turbulent models for YPL fluids, the models are far from universal. Errors found in turbulent flow data may arise from inaccuracies in the rheological model input, the turbulent modeling, or a combination of these.

Two relatively simple methods are used in this thesis to model the transitional flow regime of the fluid. They are listed below.

Model 1:

Calculates the friction factor for both the laminar and turbulent flow profiles. Laminar friction factor is calculated using Equation 2.11 and turbulent friction factor is calculated using Equation 2.12. At the Reynolds number where the turbulent friction factor is larger than the laminar friction factor, the flow is assumed to transfer from laminar to turbulent. It should be noted that this model uses a transition point not a transition region.

Model 2:

The transition region is first calculated by finding N for the fluid at the given shear rate and iteratively solving for Reynolds number using the equations below:

$$RE_1 = 3250 - 1150N \tag{2.13}$$

$$RE_2 = 4150 - 1150N \tag{2.14}$$

The resulting values are used as the boundaries for transitional flow. If the fluid Reynolds number is below RE_1, it is assumed to be laminar and Equation 2.11 is used. If the fluid Reynolds number is above RE_2, it is assumed to be fully turbulent and Equation 2.12 is used. The transition region is between RE_1 and RE_2. In the transition region, laminar and turbulent friction factors are both calculated. A weighted average is used to create the 'transitional friction factor'.

Both methods are based off of work done by Kelessidis and Dalamarinis (2011). There are many more models which can be used to calculate critical Reynolds number and friction factor (Kalayci, 2012). Throughout this thesis however, real time automation proves to be more robust than any model developed and because of this, only a brief comparative analysis is conducted.

Ahmed and Miska (2009) note that polymeric and viscoelastic fluids often extend the laminar region before flow reaches transitional flow. Rather than rely on different model values (based upon N, m, etc.) or a generic value (such as 2100), the automated pipe viscometer is able to directly calculate critical Reynolds number and friction factor values. By plotting friction factor versus Reynolds number we can easily observe the transition region for a given mud. In addition, when a Coriolis flow meter is used for measuring flow rate, one can obtain fluid density and temperature. Mud weight has a significant impact on hydraulic calculations as well as estimating the bottomhole pressure. Precise knowledge of it is therefore highly desirable.

Many empirical correlations for friction factor have been developed

which generally hold the form:

$$f = A + B(Re)^C \tag{2.15}$$

The most commonly used of these equations is the Blasius equation of the form:

$$f = 0.079(Re)^{-0.25} \tag{2.16}$$

Additional equations of the same form are shown in Table 2.1. Differences in the values attained are dependent upon the fluid tested, the limiting Reynolds numbers used in the fluid analysis, as well as general inaccuracies in experimentation (Chilton and Stainsby 1998). Errors produced from these models show the necessity of real time friction factor. Because models disagree, we propose that the best method for determining the friction factor is to create an equation of the type shown in Equation 2.15 calculated in real time from the actual data points.

Source	**A**	**B**	**C**
Blasius	0.0000	0.079	-0.250
Lees	0.0018	0.153	-0.350
Hermann	0.0013	0.099	-0.300
Nikuradse	0.0008	0.055	-0.237

Table 2.1: Table of common models used to estimate friction factor in turbulent flows (Chilton and Stainsby, 1998).

2.3 Friction Reduction

Toms and Mysels (1948) found that by incorporating a small volume of high molecular weight polymer, pressure loss in turbulent flow could be significantly decreased. Since this discovery, it has been found that many other additives can be used for friction reduction purposes including wormy micelle-forming surfactants, bubbles, rigid fibers, and solid spheres (Graham, 2004). According to Chhabra (2011), large polymer molecules confined in a narrow pipe create a low viscosity slippage layer at the pipe wall resulting in a slippage of the bulk fluid. Whether true slip occurs or not, the concept of slip has proved valuable to the analysis of polymeric fluids. The result is a much lower shear stress than expected at the assumed 'no slip' shear rate. Through the use of the automated pipe viscometer, the actual friction reduction can be determined which in turn allows for more accurate modeling during frac jobs.

Chapter 3

Equipment and Software

3.1 Experimental Setup

A major benefit of the pipe viscometer is the relative simplicity of the hardware required. The experimental setup consists of 2 pipes for pressure loss measurement (along with connecting pieces), a pump, 4 pressure sampling ports, 2 pressure sensors, a flow meter (which includes a densometer and thermometer), and a mud tank with a mixer. Figure 3.1 shows the setup of the equipment used at The University of Texas at Austin.

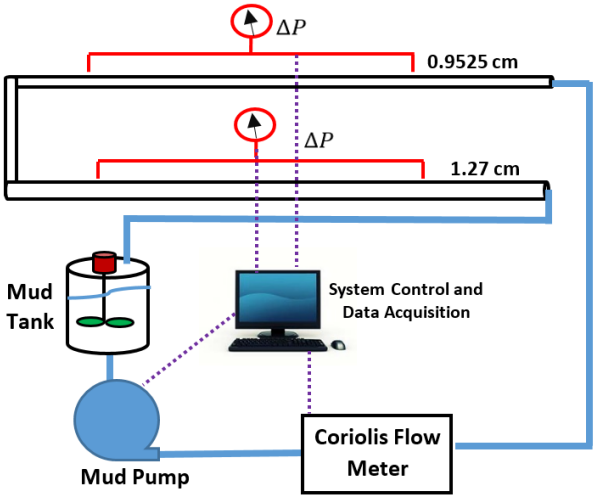

Figure 3.1: Illustration of the flow loop setup used at UT Austin for drilling fluid automation purposes.

3.1.1 Flow Pipes

The pipes used to measure pressure loss are 3/8 in (0.9525 cm) and 1/2 in (1.270 cm). The inner diameter of the pipes are approximately 0.305 in (0.7747 cm) and 0.430 in (1.0922 cm) respectively. In most cases, the smaller diameter pipe is used for turbulent flow analysis while the larger diameter pipe is used for laminar flow analysis.

Pressure ports are located 10 feet (3.048 m) apart from each other on each pipe. In addition to the length required for pressure loss calculations, an entrance and exit length are required to ensure the fluid flow profile is fully developed as it passes the sensors. The entrance and exit lengths were estimated based on empirical correlations from literature (Collins and Schowalter, 1963). The correlation used is valid for all practical drilling fluids where the fluid behavior index, $m \approx 0.2$ to 1.0. All muds tested in the system met this requirement. This length is approximated as 4 ft (1.2192 m) on each side of the pressure sensors making the total length of the system 18 ft (5.4864 m).

Of importance for the lab setup is that the flow pipes used to measure the pressure loss are horizontal, straight, and relatively smooth through the testing section. It is important to note that the pressure sensors do not need to be level, and the pipe does not need to be straight if the effects of these added variables are accounted for. A helical coil design is possible to reduce the footprint of the device on the rig site.

Additionally, a pressure relief valve was added to the setup after the

pump. The pressure relief valve was added to ensure that the pressure within the system could not exceed a safe operating level. The maximum pressure allowed in this system was set to about 250 psi (1724 kPa).

It is recommended that the smallest pipe diameters possible, without the risk of being plugged, are used in order to increase the pressure loss within the pipe. The limiting factors for the minimum pipe diameter on a rig would likely be dependent upon the mud cleaning equipment and the pump being used. Pipe diameters of about 1 in. and 3/4 in. are currently thought to be best suited for a rig. Smaller diameter pipes could likely be used in a mud building facility.

3.1.2 Pump

The pump used is a Continental Pump model 2CL6-CSQ. The pump is a progressive cavity pump, also known as an eccentric screw pump. Progressive cavity pumps are able to handle a wider range of fluid viscosities than other pumps. They work well with shear sensitive, abrasive, and viscous fluids. The rotor is able to seal tightly against the stator creating cavities that carry the liquid to the discharge port with minimal effects on fluid properties. While pumping, fluids are moved with the minimum amount of turbulence, agitation, pulsation, or separation. This minimizes changes in fluids which are thixotropic or are significantly affected by temperature.

The advertised flow range of the pump is 5 to 47 gpm and the maximum operating pressure differential across the pump is 225 psi. The pump

Figure 3.2: The progressive cavity pump used in the setup.

is controlled through a variable frequency drive (VFD) motor controller. By using the minimum allowable frequency for the pump (3 Hz), flow rates as low as 0.5 gpm were achievable when testing viscous fluids.

The pump best suited for a real world application is largely dependent upon the system setup and the environment which it is being used. Considerations for the pump when operating at rig conditions are capacity, pressure required, fluid viscosity, fluid temperature, fluid pH, operating cycle, corrosion, fluid abrasion and the amount of solids within the fluid. Two pumps may be desired if the flow rate range is insufficient for rheology and turbulent testing.

3.1.3 Flow Meter

The first flow meter used was a Badger Meter ER420 Rate Indicator/Totalizer. The flow meter consisted of a chamber with a rotating wobble disk. The biggest problem encountered with this flow meter was that the housing was made out of plastic. When solids were added to the mud, they would scratch the plastic. After sufficient scratching of the chamber and disk, fluid would slip around the measurement device leading to reading inaccuracy.

Additionally, the flow meter was unable to record values for oil based muds. It was determined that the flow meter was not sufficient for our purposes.

Figure 3.3: The Coriolis flow meter which sends 10 Hz data on volumetric flow rate, fluid density, and fluid temperature to the data acquisition center.

A Coriolis meter replaced the previous flow meter. The Coriolis meter was a MicroMotion model CMFS100M. The accuracy of the meter is extremely high (<0.1%) if the flow rate is greater than 1/20 of the maximum flow rate. For this given flow meter, the maximum flow rate is 100 gpm (6.309 l/s). If the flow rate falls below 1/20th the maximum flow rate (5 gpm) the accuracy of the flow meter worsens. A plot of this is shown in Figure 3.4. Flow rates below 1.67 gpm fall to the left of the 60:1 line shown.

In addition to flow rate, the meter is able to measure fluid density and fluid temperature in real time. Real time fluid density is important for calculating the Reynolds number of the fluid as well as the bottomhole pressure. Temperature measurements are important to ensure that the fluid properties do not change significantly during a test.

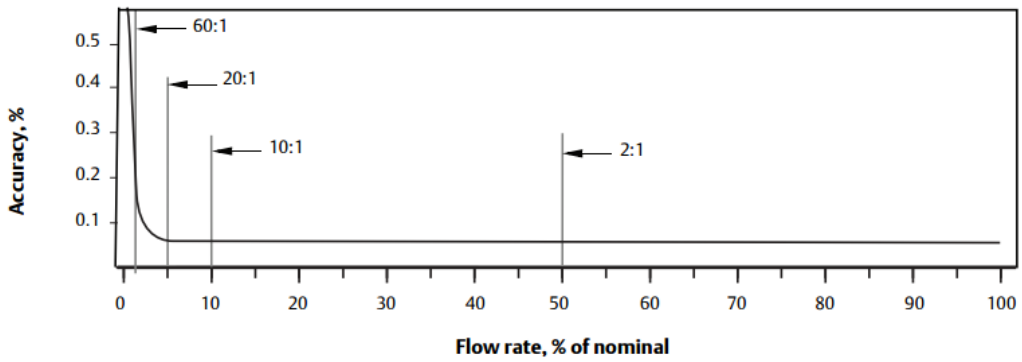

Figure 3.4: A plot of flow meter accuracy versus nominal volumetric flow rate highlighting inaccuracies at very low flow rates.

3.1.4 Pressure Sensors

T-joints, shown in Figure 3.5, were added 10 feet (3.048 m) from each other on each pipe to allow pressure measurements. The fluid pressure at the joint is transmitted to the differential pressure transducer via 1/8-inch tubing. The pressure transducer is a Rosemount 3051 transmitter as shown in Figure 3.6. The sensor line is filled with hydraulic oil during WBM tests and with water during OBM and SBM tests. This is done to keep the contents of the mud from 'caking' against the diaphragm of the pressure sensor or within the pressure transmission tubing. It was seen in early tests that if solids entered the pressure transmission tubing, they were able to prevent the transmission of pressure. The pressure sensor was designed to handle up to 300 psi (2068 kPa) differential pressure.

Pressure sensors were calibrated using a nitrogen tank with a digital pressure regulator. A maximum pressure was set for each pipe. The small

Figure 3.5: A T-joint used as a pressure sample port.

pipe was set to 200 psi (1379 kPa) maximum differential pressure and the lower pipe was set to 30 psi (207 kPa) maximum differential pressure. At this pressure, an output of 20 mA was set. The pressure differential was then removed and the amperage output at zero pressure was recorded. A linear equation ($y = mx + b$) was fit between the points. Additional points between these values were tested with an R-squared value above 0.999.

It should be noted that a fluid which will not mix with the drilling mud (i.e. oil for a WBM) is important for the pressure transmission lines. Additionally, a removable screen should likely be added to the pressure transmission line to prevent damage to the pressure transducer if solids travel along the pressure transmission lines.

Figure 3.6: Differential pressure sensor which sends data at 10 Hz to the data acquisition center.

3.1.5 Mud Tank & Mixer

The mud tank is a welded piece of aluminum able to hold about 30 liters of fluid. The mixer is a single speed mixer.

3.2 Software

The software used in these experiments was a combination of LabVIEW (for running the tests) and MATLAB (for analyzing the test results).

3.2.1 LabVIEW Software

The pump is run using LabVIEW software. The three tabs used in the software are shown below. The first tab, shown in Figure 3.7, is the opening screen of the program. This tab is where the user controls the pump. The user

can fill out the 'Frequency Setpoint' section to set a single flow rate or fill out a section of flow rates in the automatic section. The user can add as many test frequencies as desired within the automatic section. Pump input frequency and the amount of time per run can be changed as desired. By selecting 'Run Batch', the program will automatically open the MATLAB GUI, through a batch file, upon completion of the test. The MATLAB GUI is used to analyze the data, as will be discussed in the next subsection. The test is started by pressing 'Pump On'.

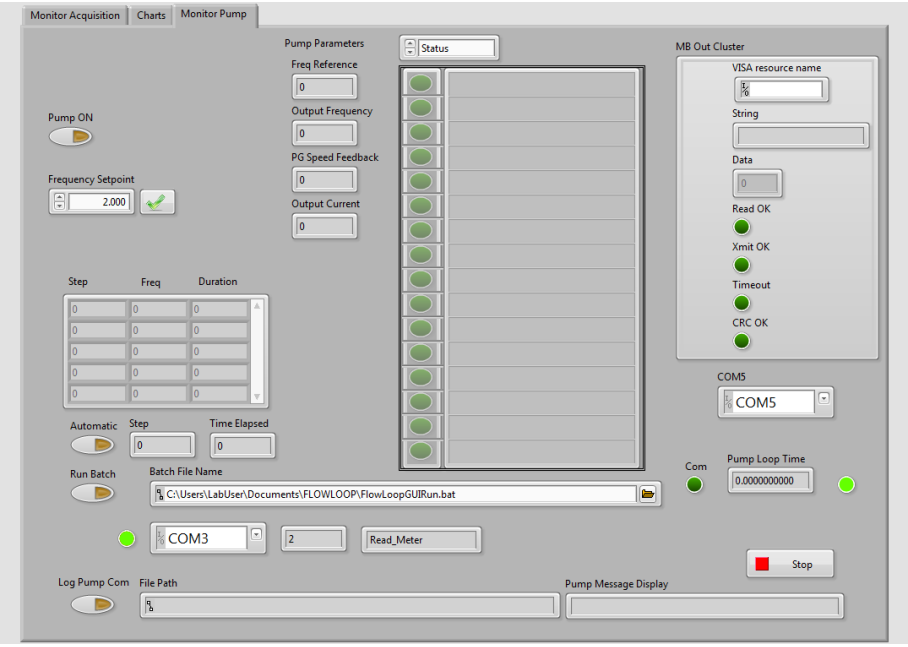

Figure 3.7: Example opening screen for LabVIEW program where pump frequency and automation are controlled.

It is important to note that frequency is used as the input for the pump. It is possible that the fluid velocity could be used as the input with a

control/feedback system but this was deemed as unnecessary for the lab setup.

The second tab, shown in Figure 3.8, allows the user to see the data being recorded during the test. Data shown includes the flow rate, density, and fluid temperature via the Coriolis meter, as well as the pressure loss in each flow pipe via the Rosemount pressure sensors. The third tab, shown in Figure 3.9, shows the data from the second tab on a single plot.

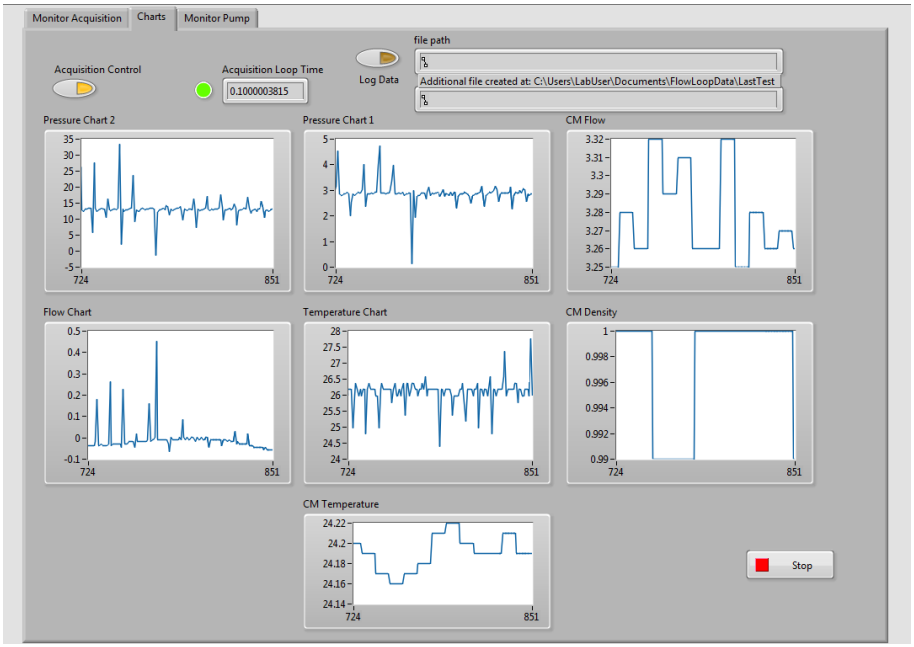

Figure 3.8: Example of individual plots to display variable changes in time.

Data from the test is saved into a .csv file of the user's choice as well as an additional .csv file in the same folder named 'LastFile. The 'LastFile' test is the default test to be run by the MATLAB GUI. The values recorded from the test include volumetric flow rate, density, pressure loss, temperature and pump frequency. All readings are recorded at a rate of 10 Hz.

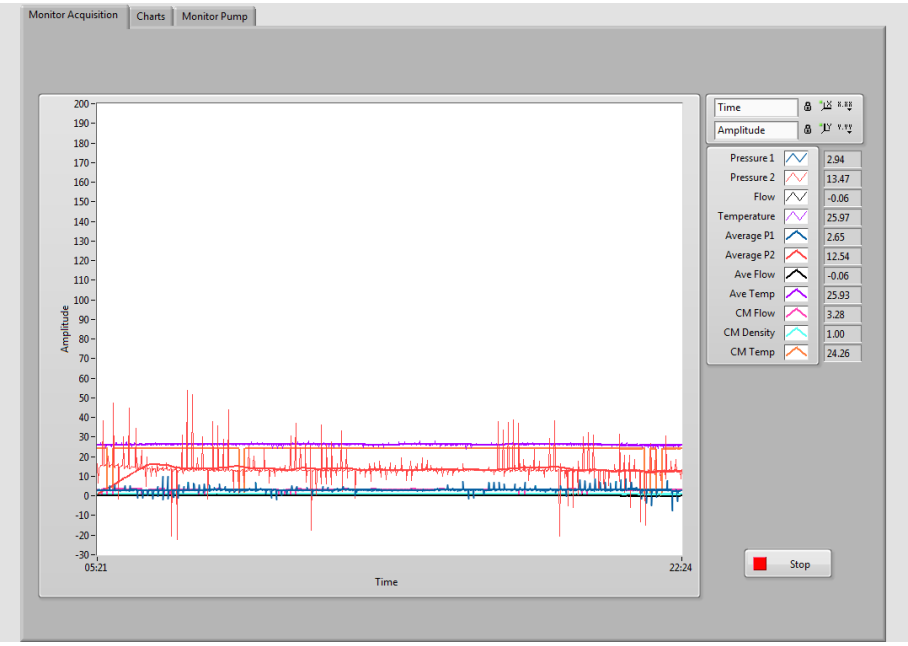

Figure 3.9: Example of the single plot containing all data recorded. Real time data and averages are shown on the right.

3.2.2 MATLAB Software

After test completion, the .csv file output from the LabVIEW program, is analyzed using MATLAB. The analysis program can be opened by selecting the 'Run Batch' option in the LabVIEW program (shown in Figure 3.7) or simply on the desktop. The GUI used for data analysis is shown in Figure 3.10. At the top of the GUI, the user is able to select the file that they would like to analyze. The default test to run is the 'LastTest' file that is overwritten by the most recent test. By choosing 'Select Another File' the user has the option to select another test for analysis from previous test results.

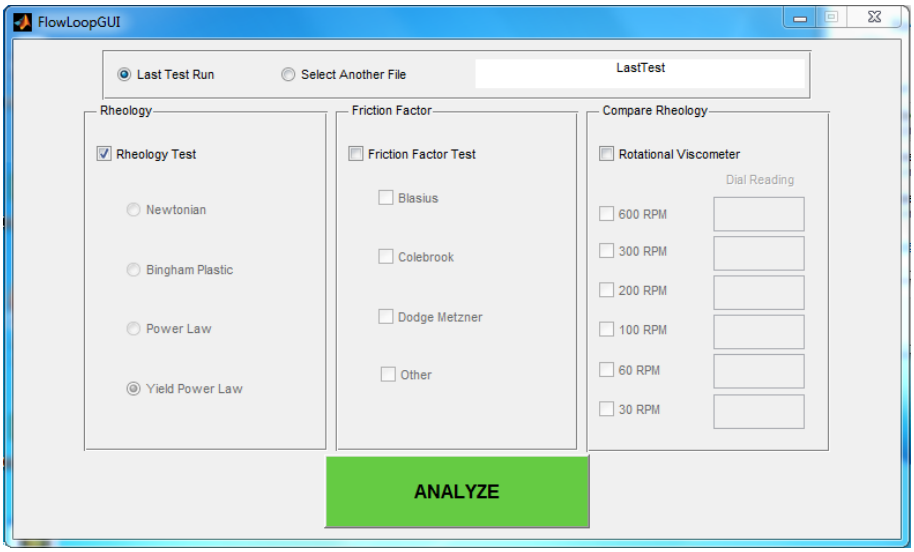

Figure 3.10: Example of Graphical User Interface from which the user selects a test and analyzation method.

The three different analyses used within the GUI are 'Rheology', 'Comparative Rheology', and 'Friction Factor'. The 'Rheology' analysis is located on the left side of the GUI. This is the only section that is default selected

upon opening the program. The user has the option to choose a given fluid model for this analysis from Newtonian, Bingham Plastic, Power Law, or Yield Power Law. The Yield Power Law model is selected by default. As discussed earlier, this model is the best fit for most drilling muds.

The 'Compare Rheology' section located on the right side of the GUI performs the same analysis as the 'Rheology' section however it also analyzes results input from the rotational viscometer. The current setup assumes that the 'Dial Readings' inputs are from an R1-B1 (standard) setup. The rheological model used to analyze the rotational viscometer is the same as the one used for the pipe viscometer.

The final analysis section 'Friction Factor' is located in the center of the GUI. The friction factor analysis can be run along with a rheological test or alone. If the friction factor test is run along with the 'Rheology' test, the parameters output from the program will be used for the friction factor analysis. If the 'Rheology' test is not selected, a prompt will appear asking the user to input the fluid rheological parameters. Currently, three different friction factor analysis can be performed; Blasius, Colebrook, and Dodge Metzner.

After pressing 'Analyze' at the bottom of the GUI, the test selected is analyzed. A total of 30 files are included in the folder to analyze the test results. Global variables are avoided in the system ensuring that running the program will not affect other computer programs. Warning dialogs, like the one seen in Figure 3.11 have been added to the program. This specific error occurred because there was insufficient data to run a turbulent flow test.

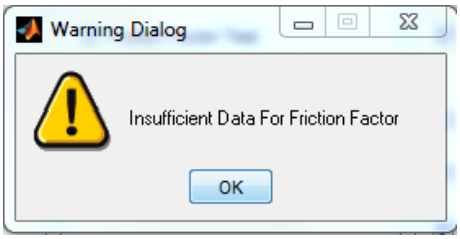

Figure 3.11: Example error message displayed if insufficient data is recorded for a given test.

A figure with four tabs is displayed when the analysis is completed. The following data should not be analyzed; it is only presented for visual purposes. The first tab, shown in Figure 3.12, shows the rheological profile of the fluid along with the data points used to create the fit. The second tab, shown in Figure 3.13, shows a comparison between the pipe viscometer values and the rotational viscometer values.

The third tab, shown in Figure 3.14, displays the friction factor of the fluid in turbulent flow. Turbulent flow can be analyzed by a user defined Reynolds number, a specific model, or a deviation from the expected laminar friction factor curve. The experimental friction factor can be compared to the friction factors developed through the Blasius, Colebrook, and Dodge-Metzner equations. The fourth tab, shown in Figure 3.15, displays the recorded pressure losses at turbulent flow rates versus the expected pressure loss from same models. From these plots, the user can clearly see how much the real pressure loss deviates from the modeled pressure loss.

Equations for the fit of every tab are displayed and saved to the computer. If the data is insufficient to create an equation, the tab shows a screen

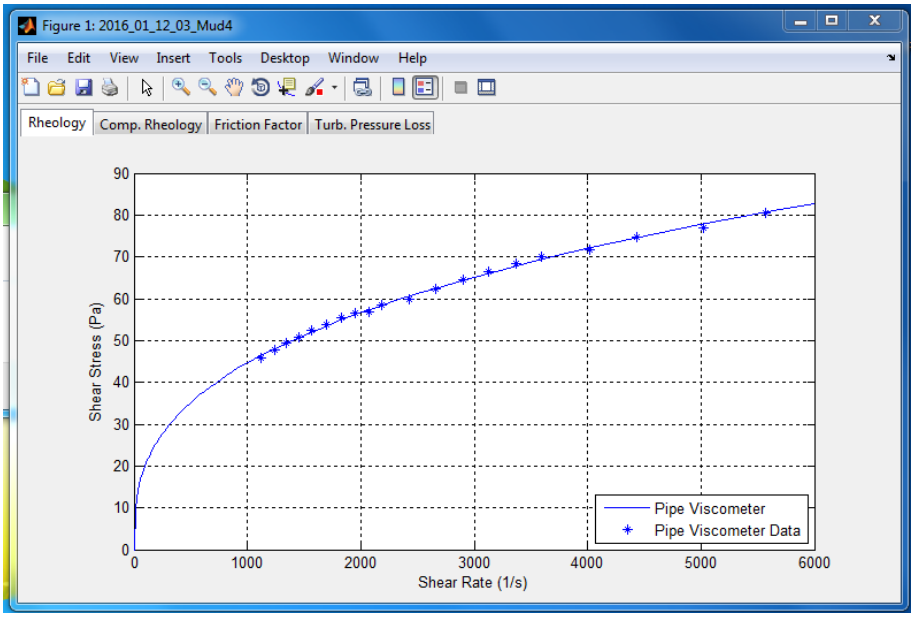

Figure 3.12: Example of first tab of output file showing the fluid rheology as measured by the pipe viscometer.

as seen in Figure 3.16.

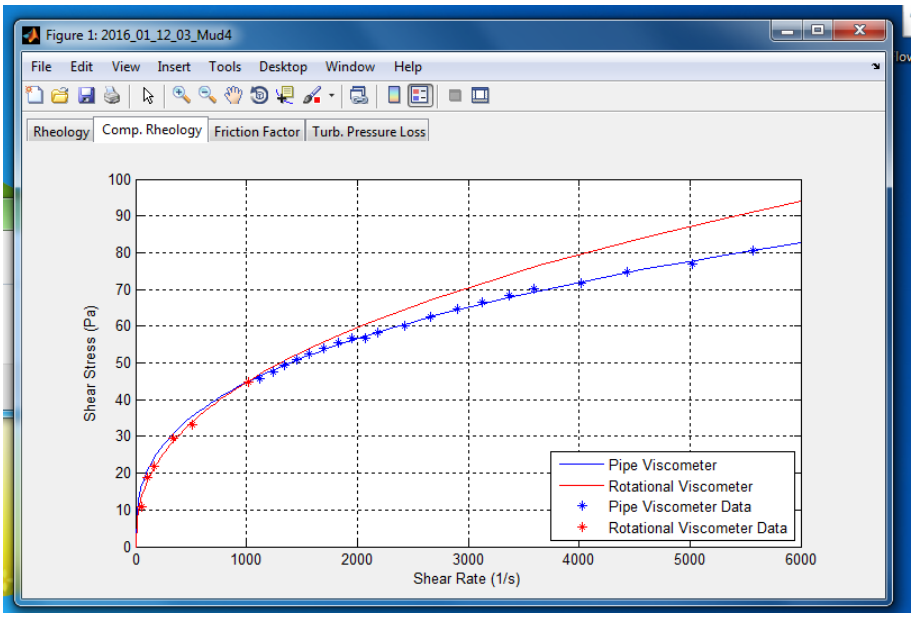

Figure 3.13: Example of second tab of output file showing the fluid rheology comparison between the pipe viscometer and rotational viscometer.

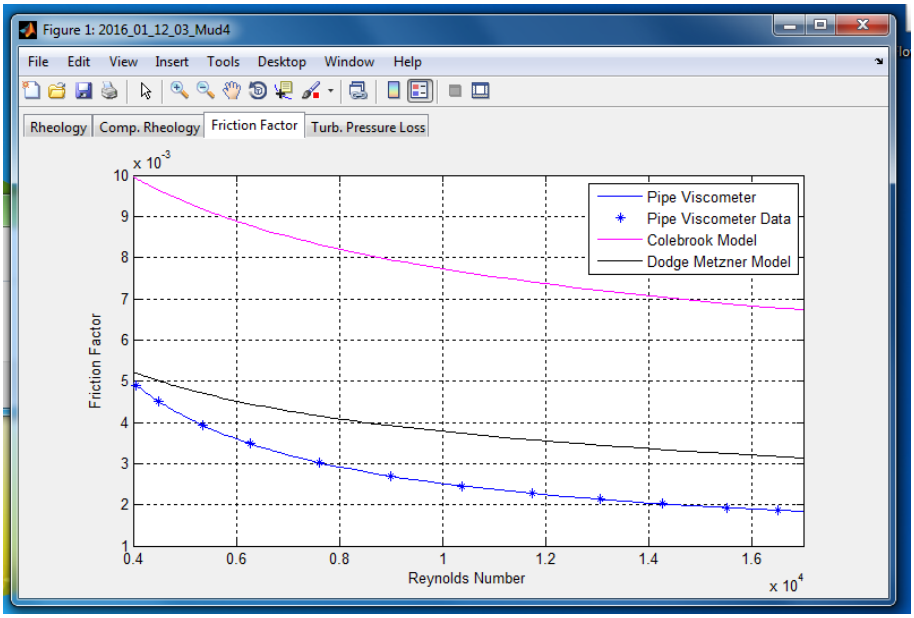

Figure 3.14: Example of third tab of output file showing friction factor versus Reynolds number. Values can be compared to additional friction factor models.

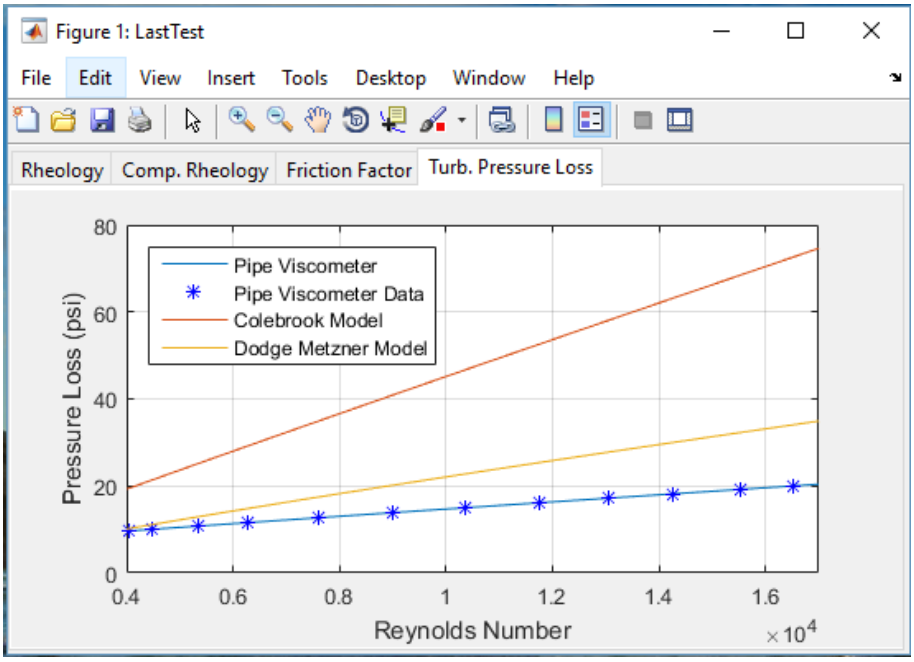

Figure 3.15: Example of fourth tab of output file showing pressure loss versus Reynolds number. Values can be compared to additional pressure loss models.

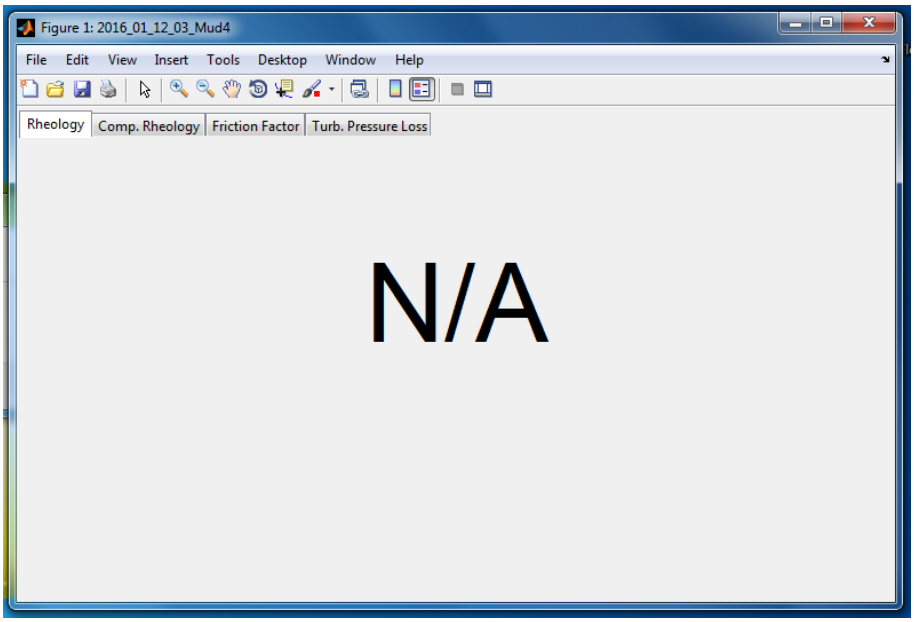

Figure 3.16: Example display screen if data is insufficient to create an analysis.

3.3 Validation of Setup

The equipment and software needed to be validated with water before tests on more complicated fluids could be performed. Figure 3.17 shows the experimental results in comparison to the pressure loss from the estimated Colebrook-White friction factor for the large pipe. The figure shows a very good match between the experimental values and the accepted model values. The smaller pipe setup is analyzed in Figure 3.18, and also shows a good match between the experimental data and modeled data.

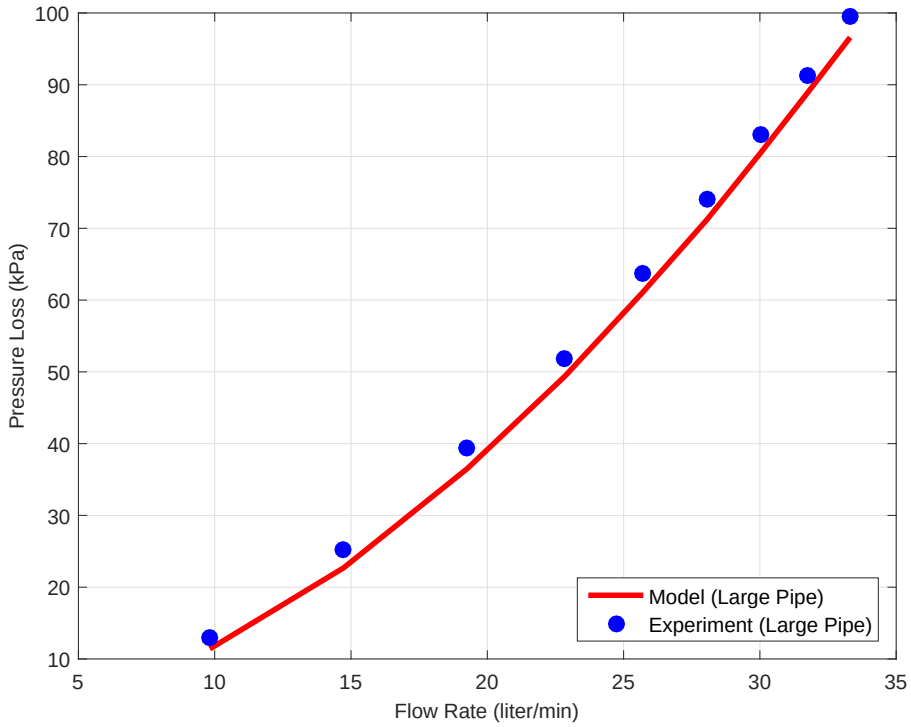

Figure 3.17: Validation of large pipe in the test setup using water. The Colebrook-White equation is used for the model.

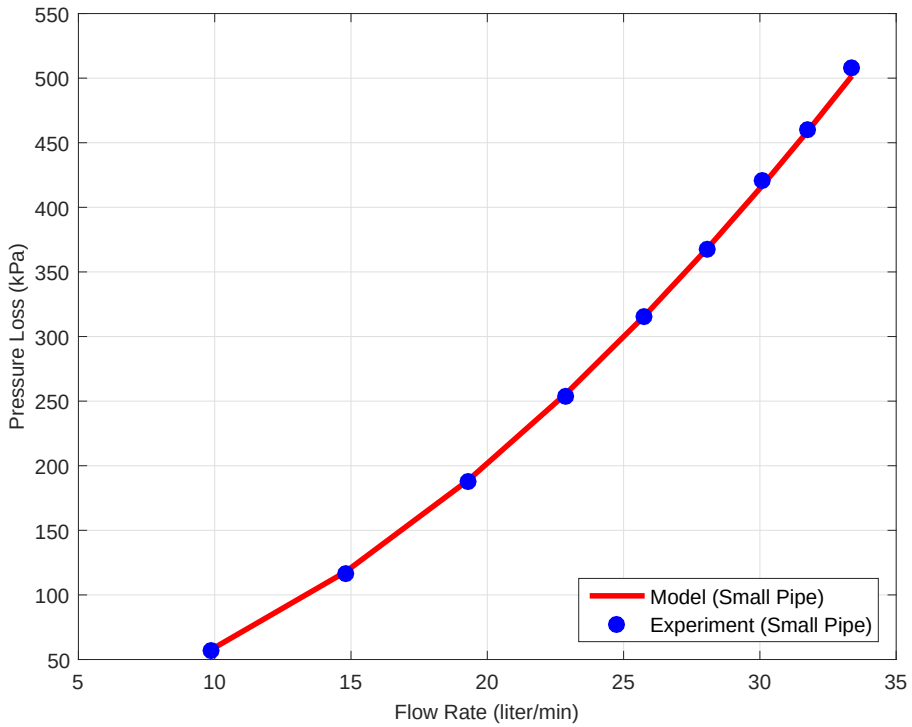

Figure 3.18: Validation of small pipe in the test setup using water. The Colebrook-White equation is used for the model.

Chapter 4

Results and Discussion

This chapter presents the experimental results and corresponding analysis for the thesis. The first two sections are separated into rheology (laminar flow) and transitional/turbulent flow. Lab designed water based muds as well as a water based field mud and a synthetic based field mud are tested. The fluid composition, as well as the basic test results for each mud are noted in Appendix A (for rheology tests) and Appendix B (for transitional and turbulent tests). The third section of this chapter analyzes friction reducers used in water and brine solutions.

4.1 Rheology

4.1.1 Mud A (Clay Based Mud)

As mentioned in Chapter 2, extensive research has already been performed on determining the rheological profile of clay based muds using a pipe viscometer. Because of this, the results in this subsection can be used as initial validation of the equations used, setup, and automation software.

Figure 4.1 shows the flow curve for Mud A. The plot shows that a quadratic type fit matches the data very well. The fit is created by an iterative

solver based upon the Curve Fitting Toolbox in MATLAB. The derivative of the function is recorded at each data point and set to the value N. Table 4.1 displays the data used for the rheology test.

All of the data shown in the table is included in determining the fit for the flow curve. The first two data points for this test (and most of the remaining tests) showed poor results and were not used in the analysis. This was assumed to be because the flow rate of the fluid was significantly below the minimum flow rate recommended for the both the pump and the flow meter. Additionally, data after reaching the transition flow regime was excluded.

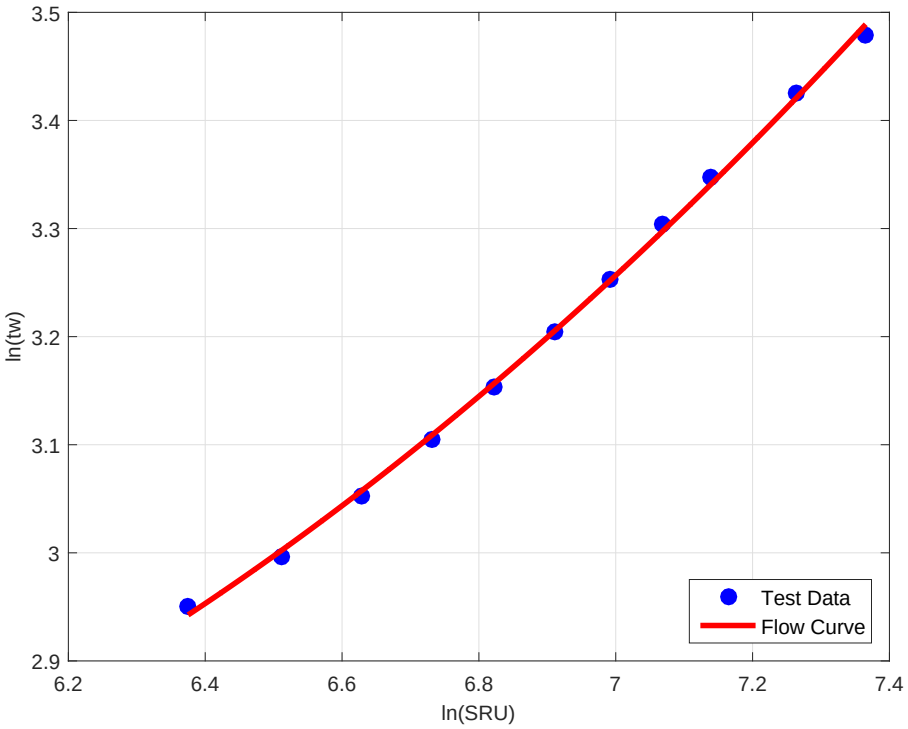

Figure 4.1: Flow curve for Mud A.

Q (gpm)	P_Loss (psi)	Vel (m/s)	dp/dl (Pa/m)	tw (Pa)	SRU (1/s)	N	y (1/s)	RE
1.37	3.2414	0.919	7332.2	20.02	673.4	0.448	880.5	386
1.53	3.4294	1.033	7757.5	21.18	756.7	0.490	953.3	465
1.70	3.6138	1.145	8174.6	22.32	838.6	0.528	1026.4	545
1.86	3.7924	1.255	8578.6	23.42	919.0	0.561	1099.2	626
2.04	3.9886	1.371	9022.5	24.64	1003.9	0.592	1176.6	715
2.21	4.1884	1.485	9474.4	25.87	1087.8	0.621	1253.5	804
2.38	4.4096	1.603	9974.8	27.24	1174.1	0.649	1332.9	899
2.55	4.6054	1.719	10417.7	28.45	1258.9	0.674	1411.1	993
2.90	4.9734	1.951	11250.1	30.72	1429.1	0.720	1568.2	1187
3.20	5.2518	2.158	11879.9	32.44	1580.6	0.756	1708.0	1364

Table 4.1: Data used for rheological profile of Mud A.

The resulting rheology from data recorded by the rotational viscometer and pipe viscometer is compared in Figure 4.2. The rotational viscometer data reaches much lower shear rates than the pipe viscometer is able to. By using a pump which is more consistent at lower flow rates or a larger pipe (to reduce fluid velocity) data closer to the values achievable by the rotational viscometer are possible. It should however, be noted that often the shear rates observed while drilling are significantly higher than the values attained by the rotational viscometer.

The rheological profiles derived by the two methods do differ slightly from each other. Table 4.2 shows the rheological fit for the fluid. Although both plots have very similar yield stresses, the rotational viscometer shows the curve to be Yield Power Law while the pipe viscometer fit appears to be very nearly Bingham Plastic. Given this data however, the relationship between shear rate and shear stress looks to be very similar when interpolating the equations.

For the given test, flow rate was held for one minute at each step.

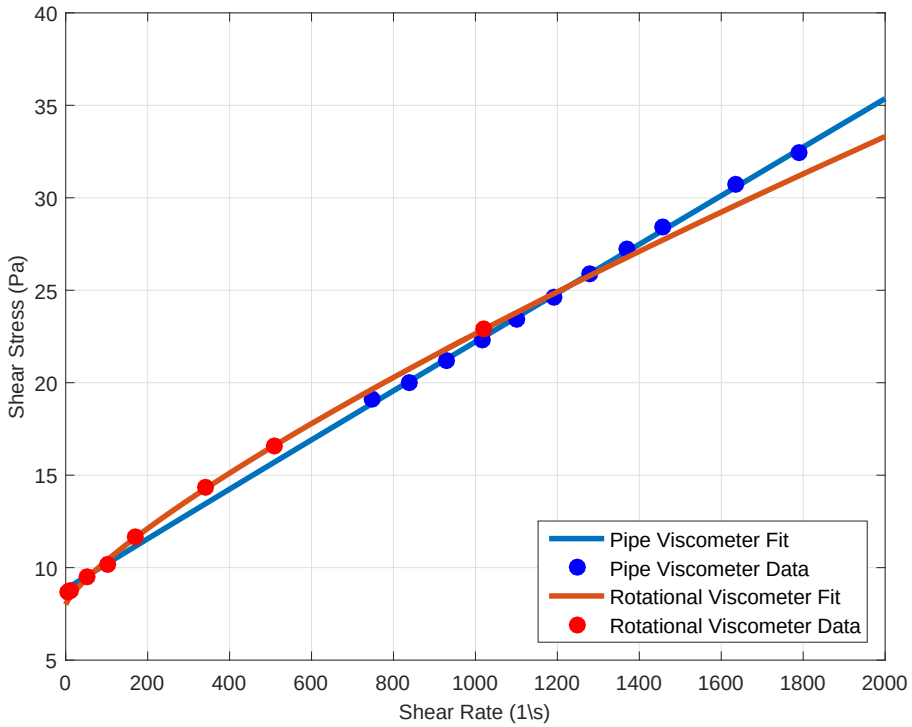

Figure 4.2: Comparison of the rheological profiles using pipe viscometer and rotational viscometer for Mud A.

Only the data collected from the large pipe viscometer was used, and the data shown in Table 4.1 was used to create the plot. A total of 11 points are used to create the rheological profile shown, meaning that this test would have taken 11 minutes to perform. It should be noted that steady state flow was achieved after 30 seconds and typically, only about 5 data points are needed to get an acceptable fit, so the test time could have been significantly reduced.

Parameter	**Rotational Viscometer**	**Pipe Viscometer**
k	0.0629	0.0146
m	0.7890	0.9876
τ_y	8.0010	8.8308

Table 4.2: Rheological profile comparison between the rotational viscometer and the pipe viscometer for Mud A.

4.1.2 Mud B (Polymer Based Mud)

The analysis of Mud B is similar to the previous analysis. After an initial iteration through the automation software, the rheology was shown to be Power Law, with a yield stress of zero. For a fluid with Power Law rheology, the flow curve will be a linear constant. A second iteration through the code with the new fit for N was performed. The new flow curve was forced to be linear, and as seen in Figure 4.3, a linear plot for N appears to be a valid approximation.

Again, all of the data shown in Table 4.3 is used to create both the flow curve and the mud rheological profile. The lowest shear rate seen during the pipe viscometer test was about 600 (1/s), lower than the lowest shear rate of

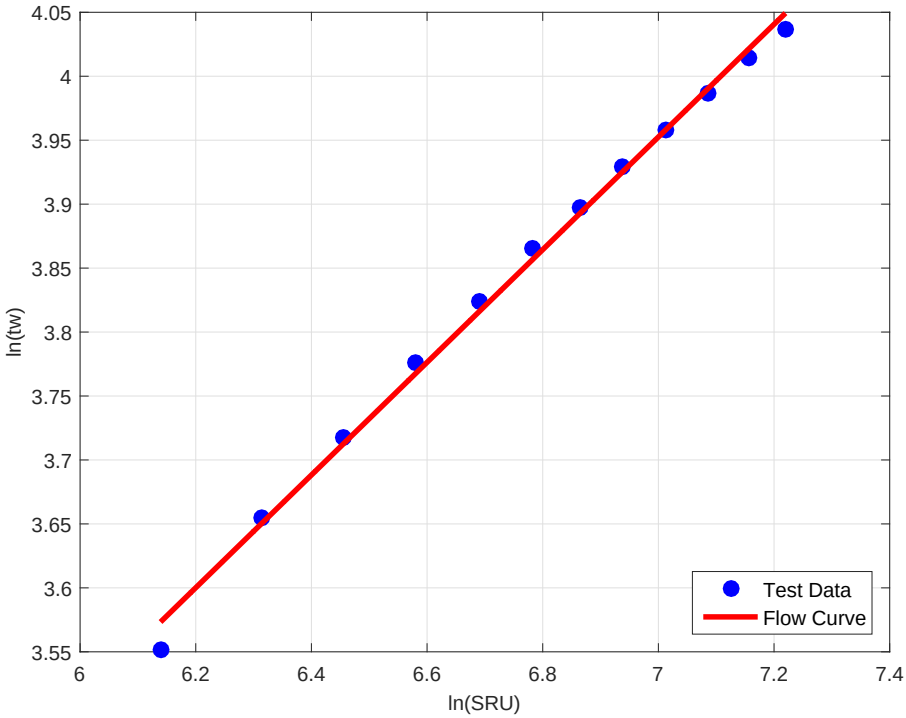

Figure 4.3: Flow curve for Mud B.

the clay based test and more comparable to the data recorded by the rotational viscometer at low shear values.

Table 4.3 shows the data used in the rheological comparison between the rotational viscometer and the pipe viscometer. Figure 4.4 shows that, the generated curves using both methods are extremely close. The Power Law fit is a suitable fit for both data sets. Table 4.4 shows the parameters for Mud B.

Q (gpm)	**P_Loss (psi)**	**Vel (m/s)**	**dp/dl (Pa/m)**	**tw (Pa)**	**SRU (1/s)**	**N**	**y (1/s)**	**RE**
0.94	5.6459	0.633	12771.4	34.87	463.7	0.441	611.0	99
1.12	6.2564	0.754	14152.3	38.64	552.5	0.441	728.0	130
1.29	6.6649	0.869	15076.4	41.17	636.4	0.441	838.4	163
1.46	7.0698	0.983	15992.3	43.67	720.2	0.441	948.9	198
1.63	7.4119	1.098	16766.2	45.78	804.1	0.441	1059.4	235
1.79	7.7237	1.206	17471.5	47.71	883.0	0.441	1163.4	273
1.94	7.9811	1.307	18053.7	49.30	957.0	0.441	1260.9	310
2.09	8.2384	1.408	18635.8	50.88	1031.0	0.441	1358.4	348
2.25	8.4775	1.515	19176.6	52.36	1110.0	0.441	1462.4	391
2.42	8.7242	1.630	19734.7	53.89	1193.8	0.441	1572.9	439
2.60	8.9645	1.751	20278.2	55.37	1282.6	0.441	1689.9	492
2.77	9.1736	1.866	20751.2	56.66	1366.5	0.441	1800.4	544

Table 4.3: Data used for rheological profile of Mud B.

Parameter	**Rotational Viscometer**	**Pipe Viscometer**
k	1.900	2.1913
m	0.4591	0.4353
τ_y	0.000	0.000

Table 4.4: Rheological profile comparison between the rotational viscometer and the pipe viscometer for Mud B.

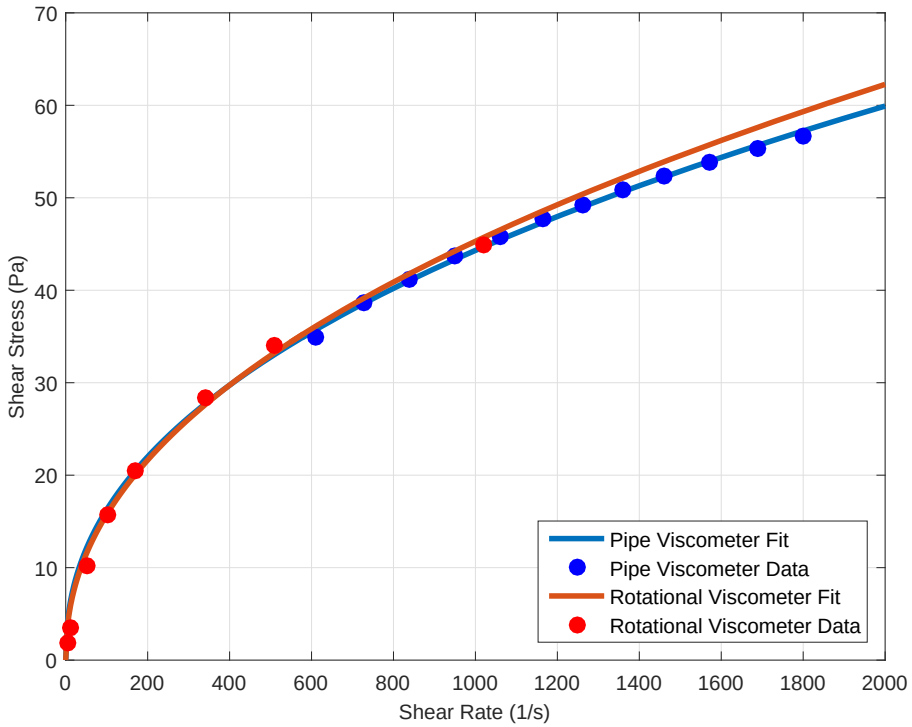

Figure 4.4: Comparison of the rheological profiles using pipe viscometer and rotational viscometer for Mud B.

4.1.3 Mud C (Synthetic Based Field Mud)

Due to the high viscosity of Mud C, much lower shear rates were achieved as seen in Table 4.5. A shear rate below 511 (1/s) (the value achieved by a rotational viscometer at 300 rpm) was achieved. This allows for a better comparison of the data between the pipe viscometer and the rotational viscometer.

Q (gpm)	P_Loss (psi)	Vel (m/s)	dp/dl (Pa/m)	tw (Pa)	SRU (1/s)	N	y (1/s)	RE
0.80	3.6427	0.541	8240.0	22.50	396.1	0.675	443.8	135
0.95	4.1563	0.639	9401.8	25.67	468.2	0.686	521.7	167
1.11	4.836	0.744	10939.3	29.87	545.1	0.697	604.3	201
1.26	5.3135	0.851	12019.5	32.82	623.5	0.706	688.3	237
1.42	5.8082	0.956	13138.5	35.87	700.5	0.715	770.4	273
1.59	6.307	1.070	14266.8	38.96	783.4	0.722	858.6	313
1.76	6.7927	1.184	15365.5	41.96	867.2	0.730	947.6	354
1.93	7.2476	1.301	16394.5	44.77	952.6	0.736	1037.9	396
2.10	7.6617	1.416	17331.2	47.32	1036.9	0.742	1127.0	439
2.27	8.0835	1.528	18285.4	49.93	1119.3	0.747	1213.9	482
2.43	8.5216	1.634	19276.4	52.63	1196.8	0.752	1295.4	522
2.74	9.4242	1.847	21318.1	58.21	1353.2	0.761	1459.6	605
3.04	10.2207	2.047	23119.8	63.13	1499.2	0.768	1612.5	684

Table 4.5: Data used for rheological profile of Mud C.

The flow curve shown in Figure 4.5 is very nearly linear. The first two data points recorded were removed from the flow curve plot. The data points appeared to be significantly below the trend of the other data and determined incorrect. Figure 4.6, shows the rheology follows a Power Law rheology. As we noted with Mud B, Power Law fluids show a nearly constant N value for the flow curve. The curve being nearly linear is a sign that the flow curve is correct. Table 4.6 compares the parameters attained using both viscometers.

As noted earlier, due to the mud viscosity, a lower shear rate could be achieved. This shear rate could be further reduced by using larger pipes or a

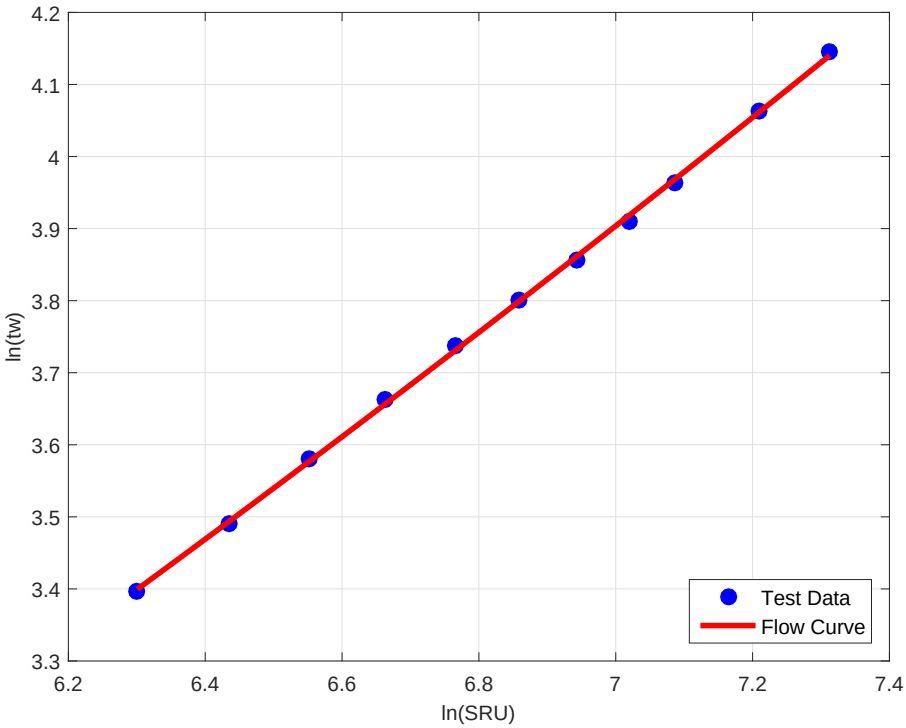

Figure 4.5: Flow curve for Mud C.

pump that was meant for lower flow rates. The directly comparable results, for the final two rotational viscometer points, at 300 and 600 rpm, the pipe viscometer shows a very good match. Aside from the slight difference at 600 rpm, the two rheologies are almost identical. By reducing the shear rate, we can see that we have a better understanding of the yield stress for the fluid.

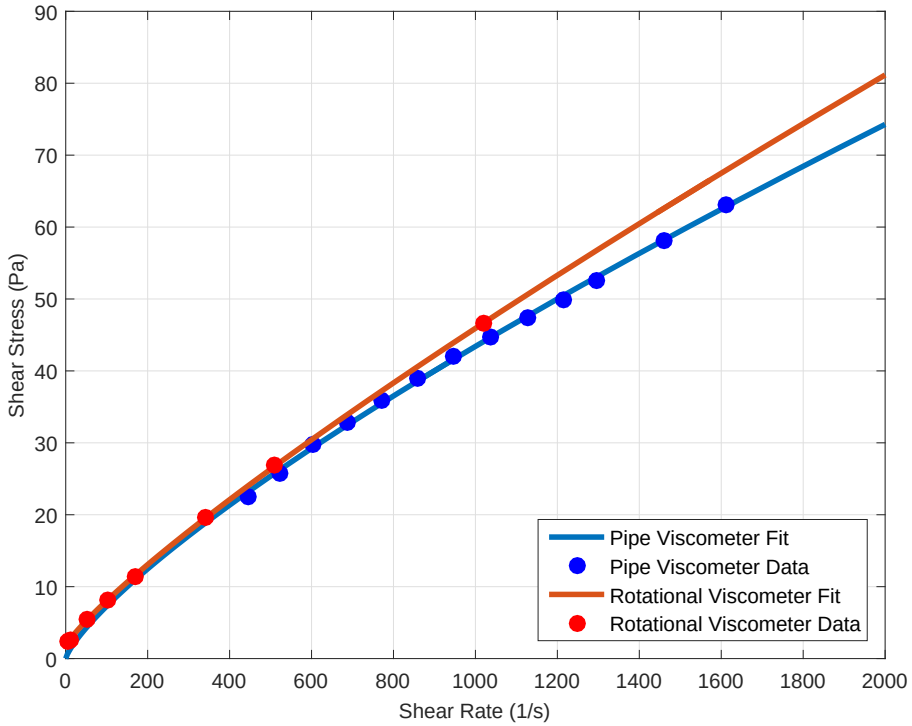

Figure 4.6: Comparison of the rheological profiles using pipe viscometer and rotational viscometer for Mud C.

Parameter	Rotational Viscometer	Pipe Viscometer
k	2.209	0.2056
m	0.3995	0.7748
τ_y	0.000	0.000

Table 4.6: Rheological profile comparison between the rotational viscometer and the pipe viscometer for Mud C.

4.1.4 Real Time Rheology

During drilling operations, mud properties can go unchecked for very long periods. Within this time, fluid property changes caused by influxes, mud shearing, mud temperature changes, etc. can go unnoticed. Through the use of the automated pipe viscometer, fluid changes can be quickly accounted for and the associated problems can be avoided.

An 'influx' was added to Mud A. The influx contained about 4 lb/bbl bentonite and about 15 lb/bbl rev dust. The change in rheological profile can be seen in Figure 4.7. Mud properties are shown in Appendix A for Mud A*.

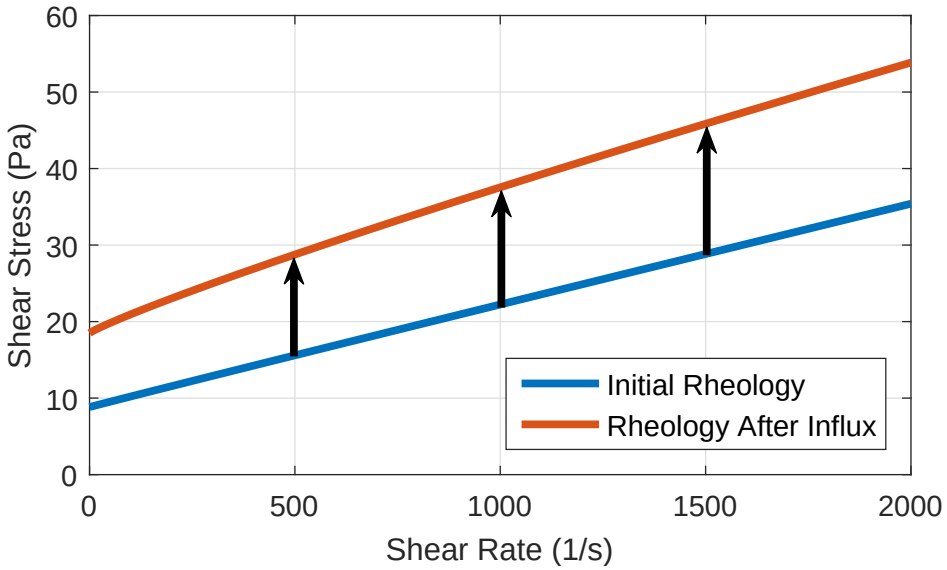

Figure 4.7: Plot showing the rheological change in the mud caused by the influx.

4.2 Transitional and Turbulent Flow Analysis

The muds used in Section 4.1 were too thick to achieve sufficient Reynolds numbers for turbulent analysis. Thinner muds were developed for transitional and turbulent testing.

Analysis of the experimental turbulent friction factor is set to fit Equation 2.15. Turbulent flow is assumed after an inflection point in the data showing the decrease in friction factor slowing in comparison to Reynolds number. This usually occurred after a quick increase in friction factor during transitional flow.

Temperature changes and additional shearing during a test affect the

rheological values of the mud. Because of this, the rotational viscometer readings found after the test were used to more closely match the fluid temperature during the test.

Rheological parameters were obtained after the test using an OFITE Model 900 rotational viscometer.

An area of major importance is at what Reynolds number flow will transition from laminar (critical Reynolds number) and when it will reach fully turbulent flow. The critical Reynolds number is most easily found by calculating the model friction factor using Equation 2.11 and comparing these values to the experimental friction factor data. When the friction factor deviates from this equation (which is not a perfect fit) the fluid is considered to be entering transitional flow. Additionally, critical Reynolds number can be found by plotting $\Delta\ P$ versus Q or τ_w versus $8v/D$ and observing a deviation from the rheological profile.

Because the transition regions of the muds vary significantly, a simple linear fit is used between each point. If the readings are taken at sufficiently high resolution, this is the most accurate and robust way to calculate the friction factor within this complex region. It is assumed that a cubic curve fit is often the best model for the transitional friction factor versus Reynolds number.

The two models discussed in Chapter 2 are used in this analysis.

4.2.1 Mud D (Clay Based Mud)

Previous research on pressure loss of Yield Power Law fluids is centered around clay based muds. Similar to the rheology tests, the clay based fluid will be used as a baseline test. The test spanned flow rates from 0.92 to 7.39 gpm and Reynolds numbers from about 470 to about 7200. The mud weight was 9.50 ppg. Figure 4.8 shows a very good match between the experimental data and the model used. The rheological values attained using the pipe viscometer were slightly lower than expected. Friction factor values using the Dodge-Metzner formula are very close to the experimental results as expected, and it can be said that the model accurately represents the fluid.

Although the turbulent flow is well represented by the model, the transitional flow, as seen in Figure 4.9, is not. The first model, predicts a transition region beginning at a flow rate of 2.07 gpm. It is obvious from the data that the transition point occurs after this. The second model finds a transition region from 3.25 to 4.10 gpm. It can be seen that the transition region occurs before these flow rates.

Figure 4.10 gives a clearer representation of the friction factor versus Reynolds number. The magenta line represents the expected friction factor based upon the standard Fanning friction factor in laminar flow.

Creating a fit for the turbulent model was more complicated. The data show an increase in friction factor at a Reynolds number of about 2000. After this point, an inflection point was found at a Reynolds number of about 3400.

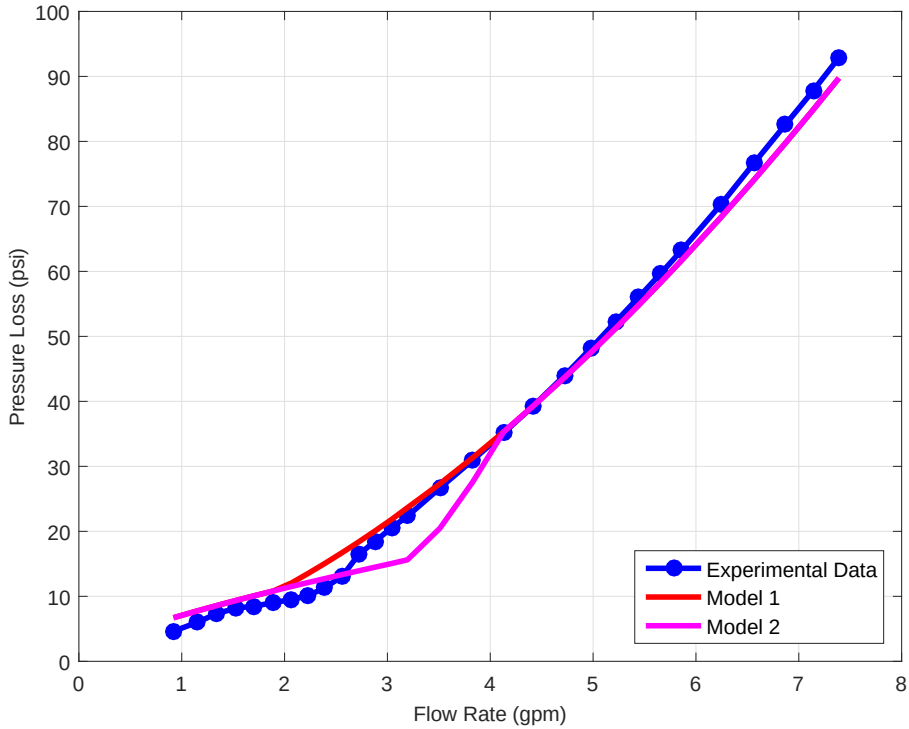

Figure 4.8: Comparison between values obtained from experimental data and the models for Mud D.

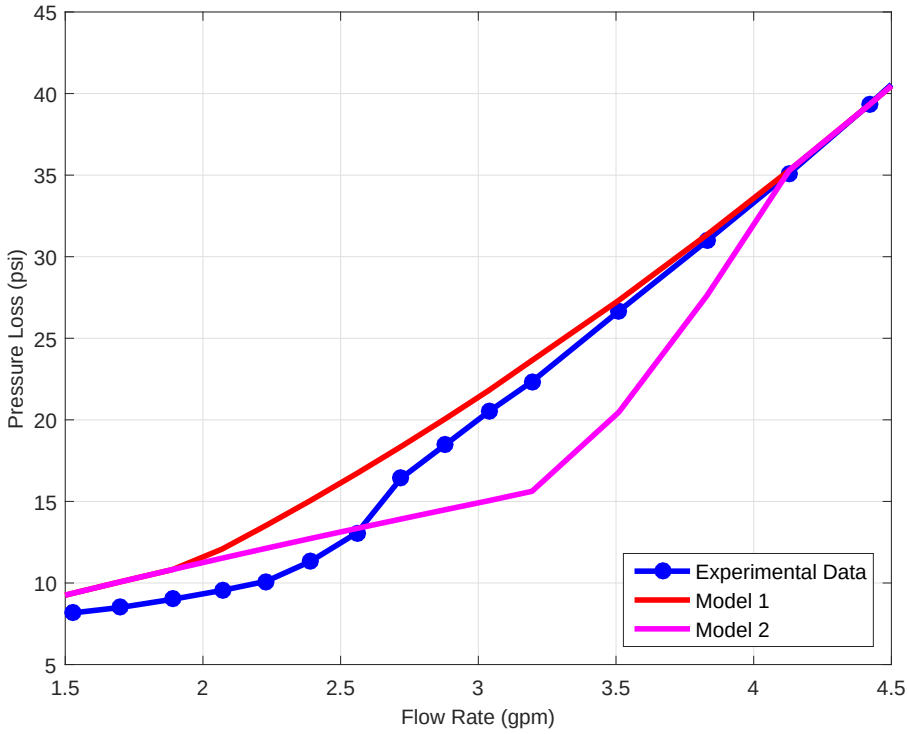

Figure 4.9: Transitional comparison between values obtained from experimental data and the models for Mud D.

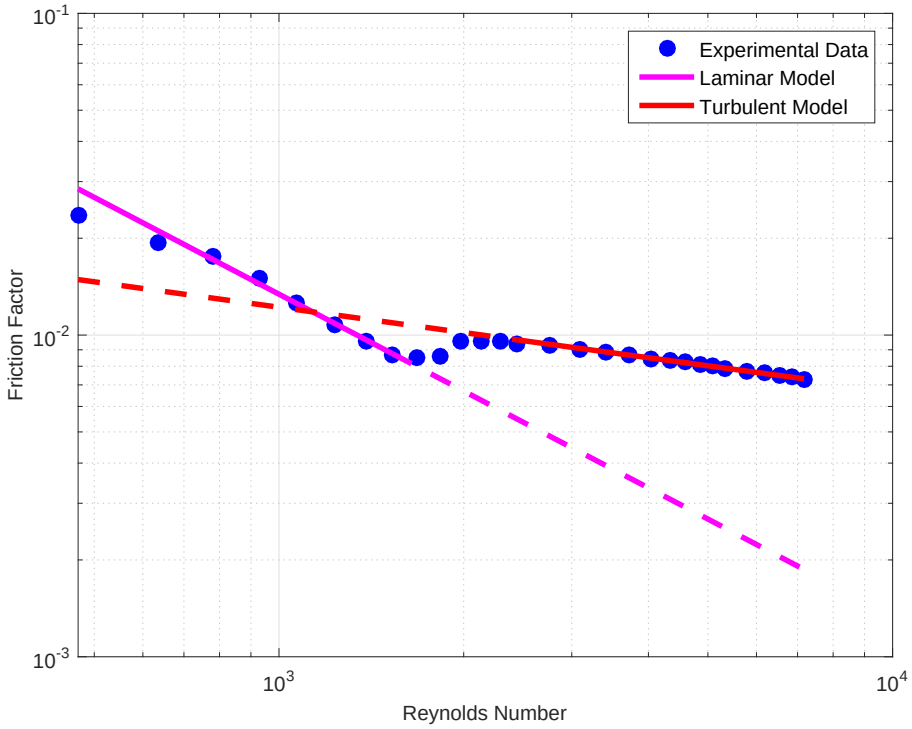

Figure 4.10: Friction factor versus Reynolds number for Mud D.

It is assumed that at this point the flow is fully turbulent. A curve fit of the type in Equation 2.15, was developed for this section of data. As expected, this equation is a nearly perfect match for the turbulent data. The resultant parameters are shown in Table 4.7 (in Section 4.2.6).

Figure 4.11 shows the transition region of the mud. As discussed, a line segment is created to attach each point within this region. The transition point in this fluid is from a Reynolds number of about 1500 to 2500. A major increase in friction factor is seen between Reynolds numbers of 1800 and 2000.

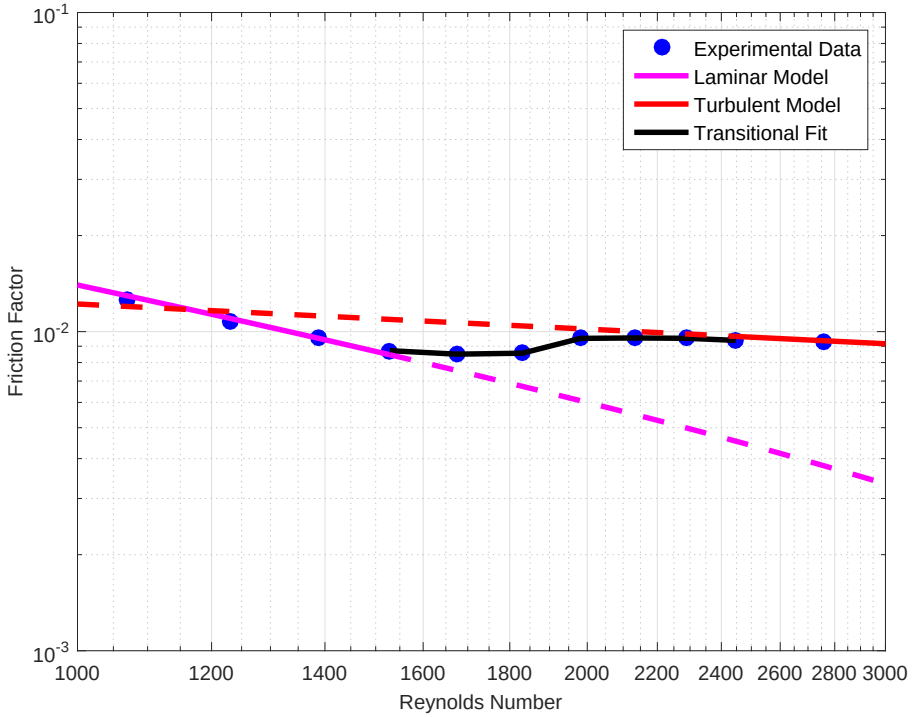

Figure 4.11: Transitional friction factor versus Reynolds number for Mud D.

4.2.2 Mud E (Polymer Based Mud)

The transitional and turbulent pressure loss were measured in Mud E to see if the results differ from Mud D. From the literature review, the transitional and turbulent pressure loss in the pipe for a polymer mud are expected to be much lower than the estimate provided by the Dodge-Metzner equation. As we can see in Figure 4.12, our assumption is correct and the friction factor is much lower than the value estimated by the Dodge-Metzner formula. Flow rate varied from 0.93 to 10.75 gpm and Reynolds numbers ranged from about 600 to 29000. The mud weight was 9.33 ppg.

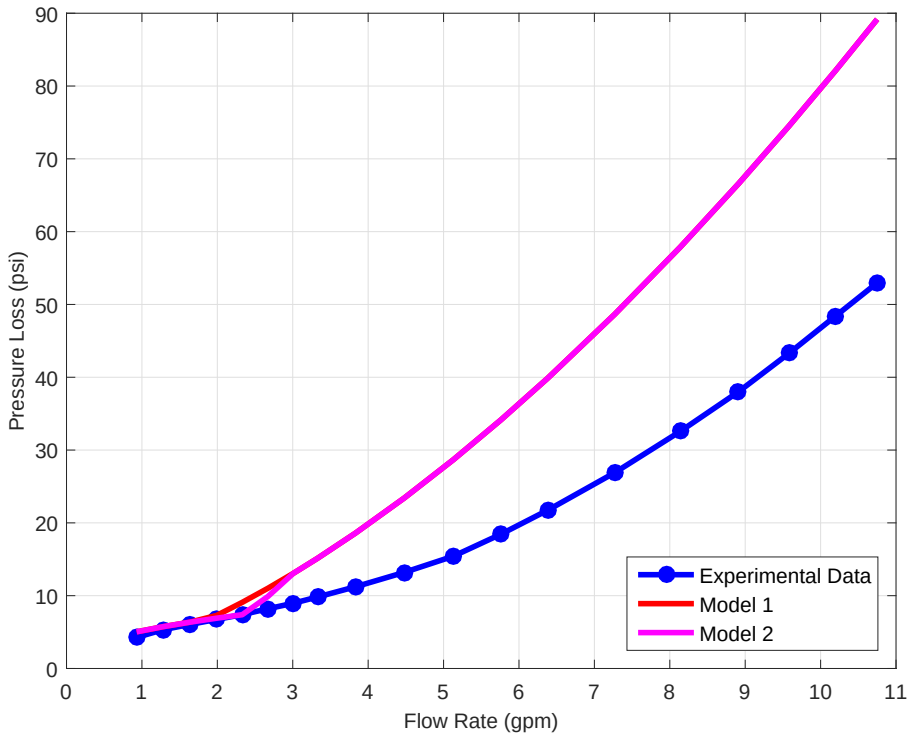

Figure 4.12: Comparison between values obtained from experimental data and the Dodge-Metzner for Mud E.

Although the turbulent data does not match the model, the laminar values, still do. Figure 4.13 shows a plot of the experimental friction factor against the Reynolds number. It can be seen that for this fluid there is not a spike in friction factor as seen for the clay based mud. In fact, the transition from laminar to turbulent flow is very smooth. The friction factor begins to deviate from the laminar flow model at a Reynolds number of about 3300. Because the Dodge-Metzner model is not close to the experimental data, the transitional data is obviously incorrect.

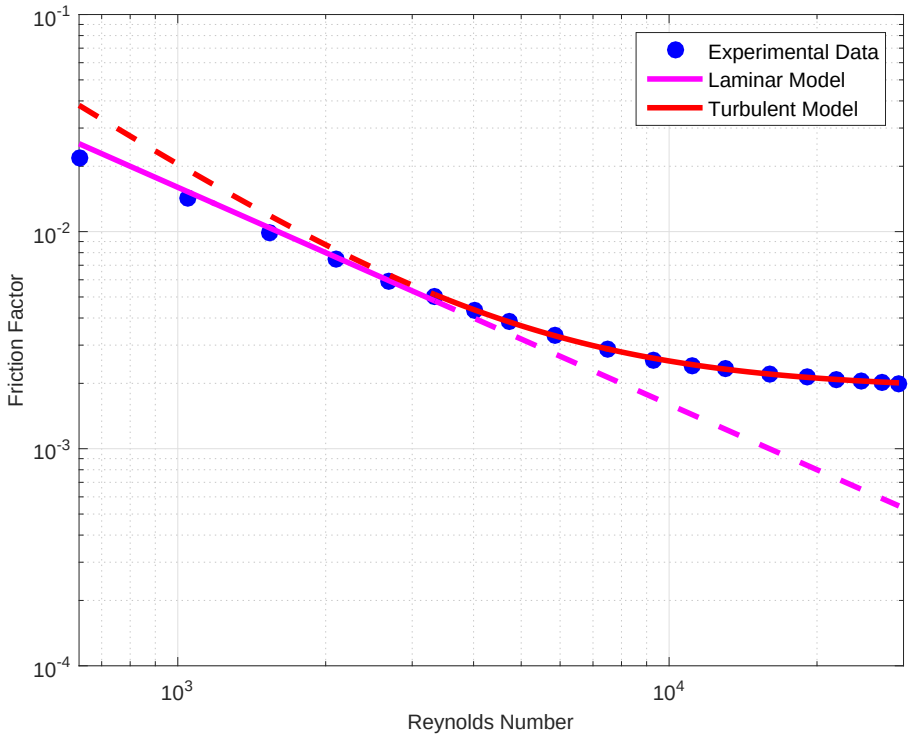

Figure 4.13: Friction factor versus Reynolds number for Mud E.

There is no inflection point in Figure 4.13 and because of this, the

turbulent flow rate was started immediately following the laminar flow rate at a Reynolds number of 3300. As we can see, the friction factor decreases very slowly with Reynolds number. Due to the flexibility of the model, it is able to match the curve very well. The parameters, shown in Table 4.7 show that the fluid differs significantly from all others tested in turbulent flow.

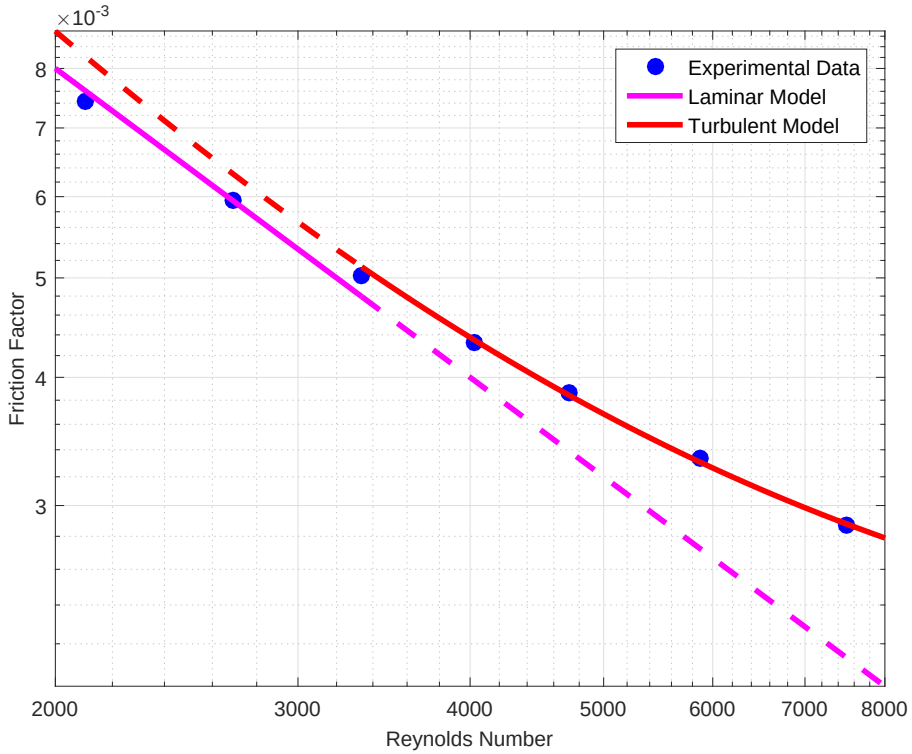

Figure 4.14: Transitional friction factor versus Reynolds number for polymer based mud.

A second test to observe the effects of long-term shear on polymer degradation was run. The mud was sheared at a Reynolds Number of approximately 10,000 for 8 hours. The flow rate was reduced as temperature approached 40 °C to ensure that the polymer was not degrading due to tem-

perature increase. After shearing, another pressure loss test was performed. As can be seen in Figure 4.15 the two curves do not match at high flow rates (high turbulence). The tests were both started at about 29 °C. Degradation in the mud could have been caused by the mud shearing or the elevated temperature seen for an extended period of time. Regardless, the change in turbulent friction factor shows why all fluid models have problems, and why real time friction factor is so important.

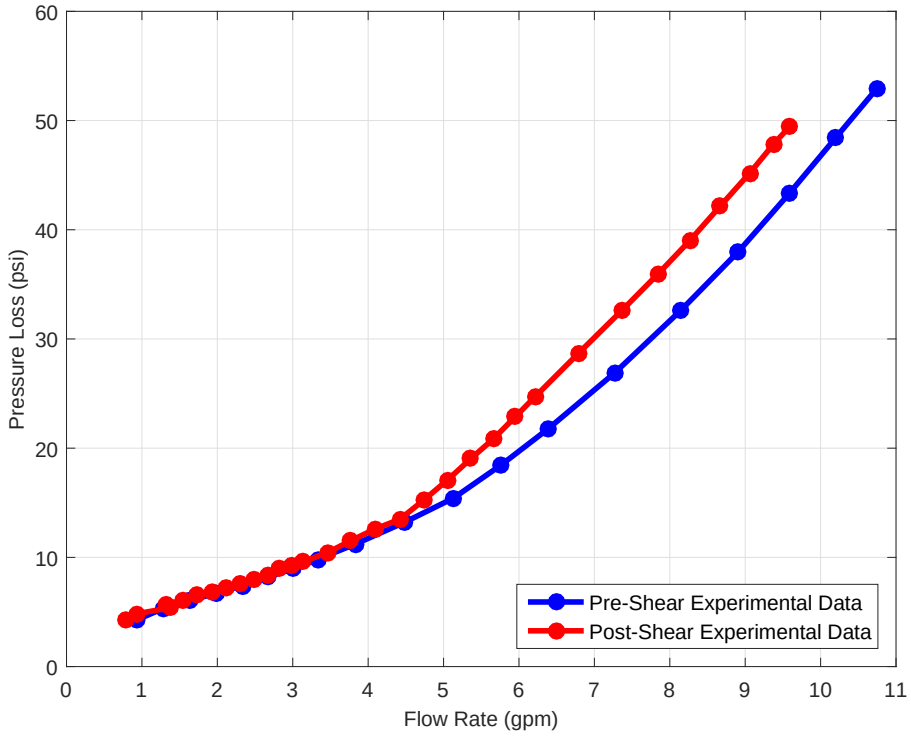

Figure 4.15: Plot of pressure loss versus flow rate before and after shearing mud for an extended period.

4.2.3 Mud F (Clay and Polymer Based Mud)

Mud F was made containing both polymers and clay to determine the effect on friction factor. Initial predictions were that the friction factor would be reduced in turbulent flow due to the presence of polymers. However, instead of showing the friction reduction properties expected in a mud containing polymers, the fluid acted very similar to the entirely clay based mud. Flow rates varied from 1.28 - 8.84 gpm and Reynolds number of approximately 1300 to 15500. The mud weight used was 9.08 ppg.

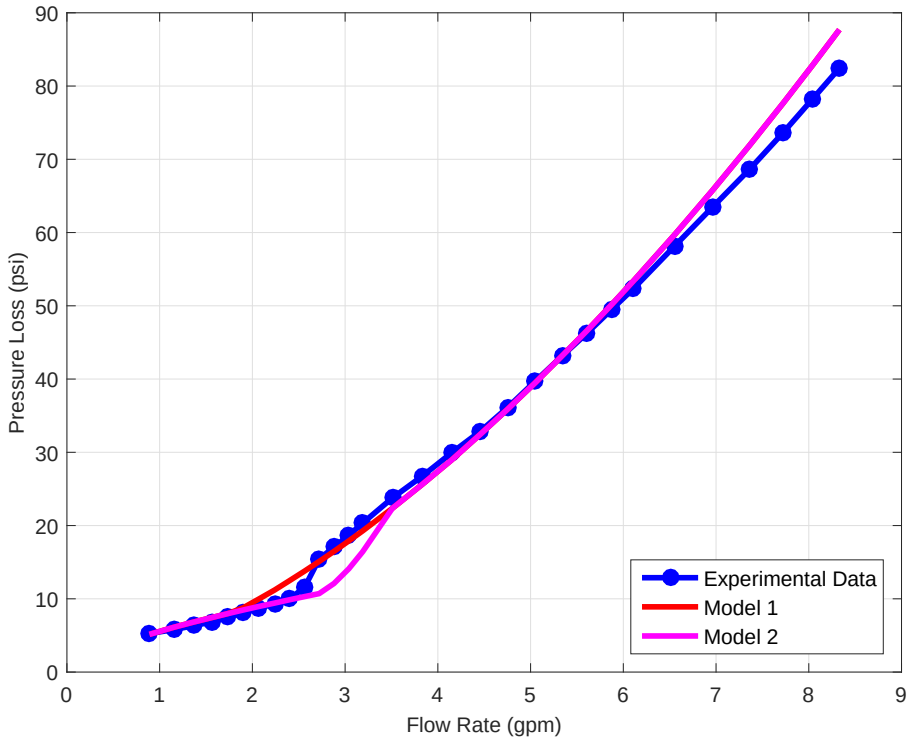

Figure 4.16: Comparison between values obtained from experimental data and the Dodge-Metzner for Mud F.

Figure 4.16 shows the experimental data versus the models for Mud F.

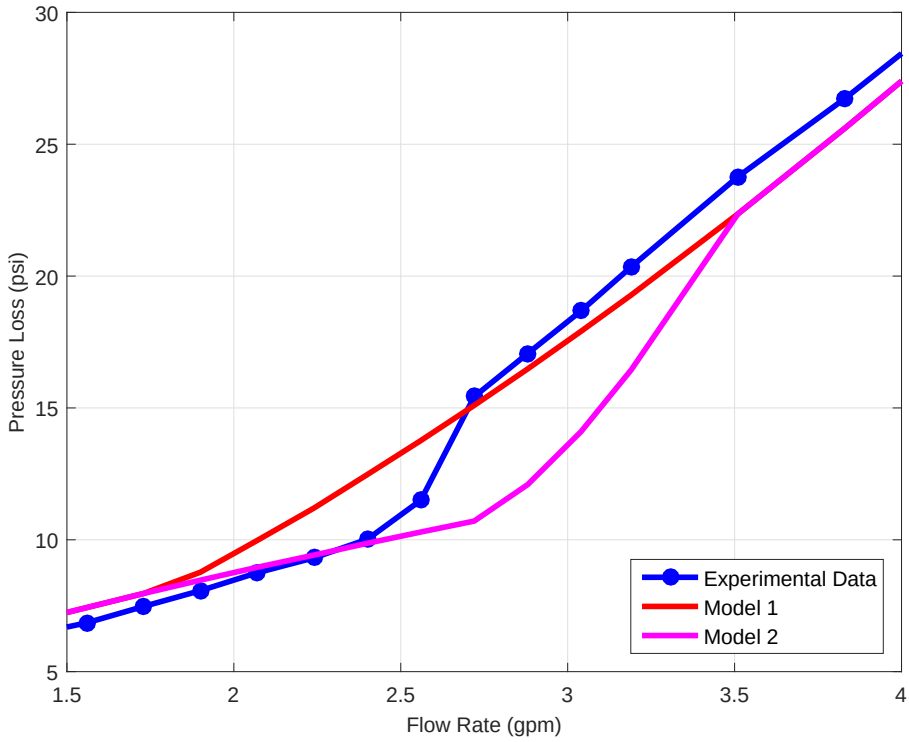

Figure 4.17: Transitional comparison between values obtained from experimental data and the Dodge-Metzner for Mud F.

Again, the model matches the experimental data well at laminar flow rates, and at turbulent flow rates. The experimental pressure loss begins to slightly deviate from the model data at very high Reynolds numbers. Figure 4.17 shows that again, Model 1 predicts that the transition point will occur too soon, and Model 2 predicts that the transition region will occur too late.

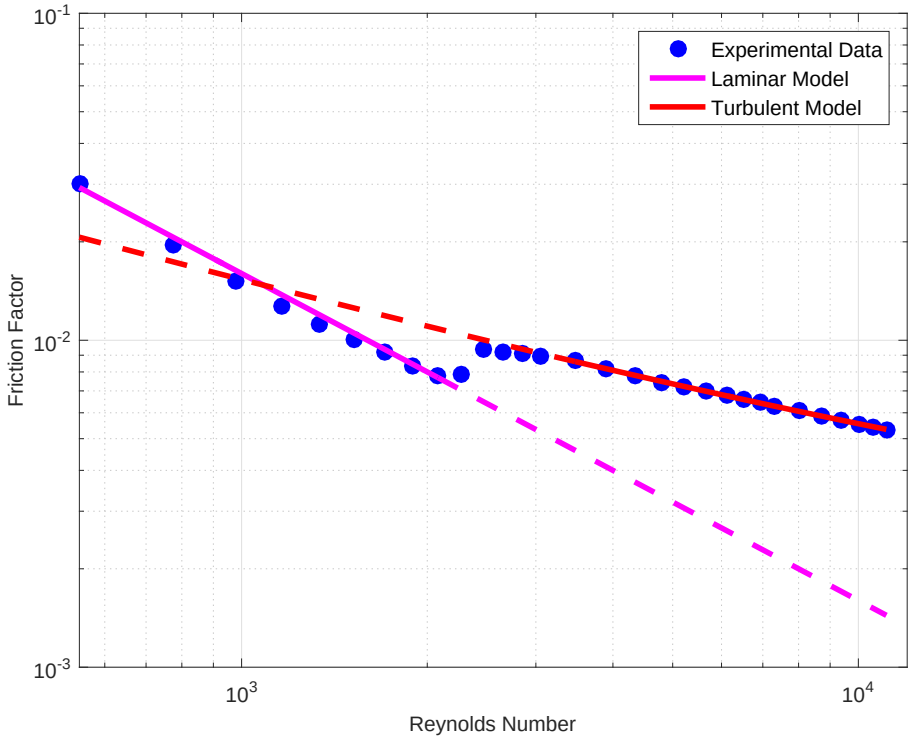

Figure 4.18: Friction factor versus Reynolds number for Mud F.

Experimental friction factor is plotted against Reynolds number in Figure 4.18. An increase in friction factor is seen at a Reynolds number of about 2500. After this point, an inflection point is seen at Reynolds number of about 3900. An equation for turbulent friction factor was developed from this point

to higher Reynolds numbers. After fitting a curve, the turbulent model was fit to the data. The point at a Reynolds number of about 3500 was found to be sufficiently represented by the turbulent equation and set as the initial turbulent point.

Figure 4.19 shows the transitional fit for the mud. The transitional section begins at a Reynolds number of about 2100 and ends at a Reynolds number of 3500. These values are close to the commonly accepted values for transitional flow.

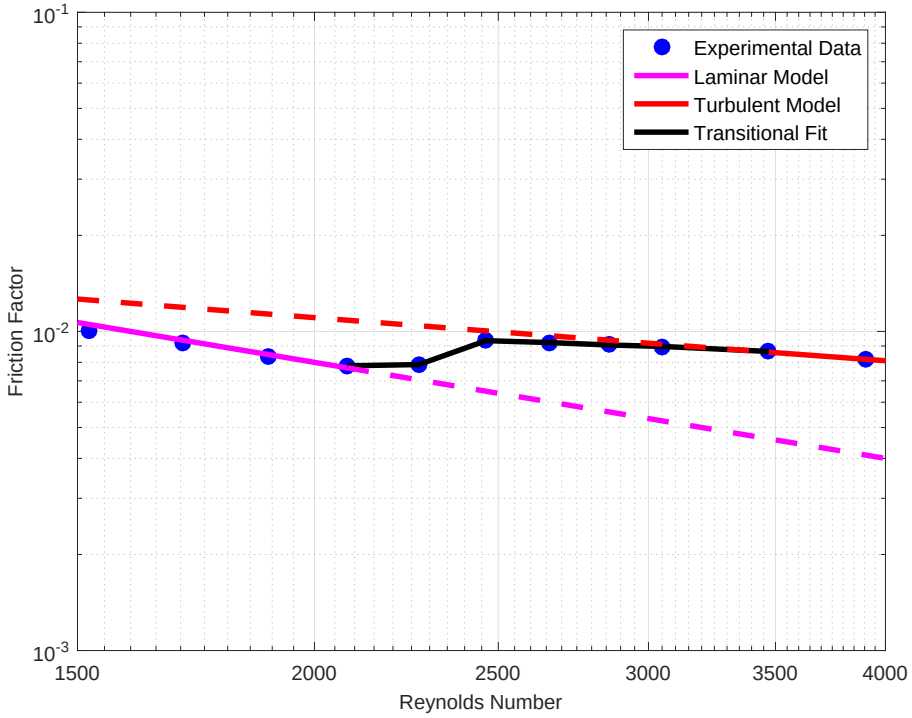

Figure 4.19: Transitional friction factor versus Reynolds number for Mud F.

4.2.4 Mud G (Water Based Field Mud)

A water based field mud was provided by a drilling company and tested for friction factor properties. The original mud was diluted with tap water to 10.5 ppg in order to achieve a sufficient pressure drop with given pump limitations. The flow rates achieved ranged from 0.88 to 7.98 gpm with Reynolds number varying from about 700 to 17000.

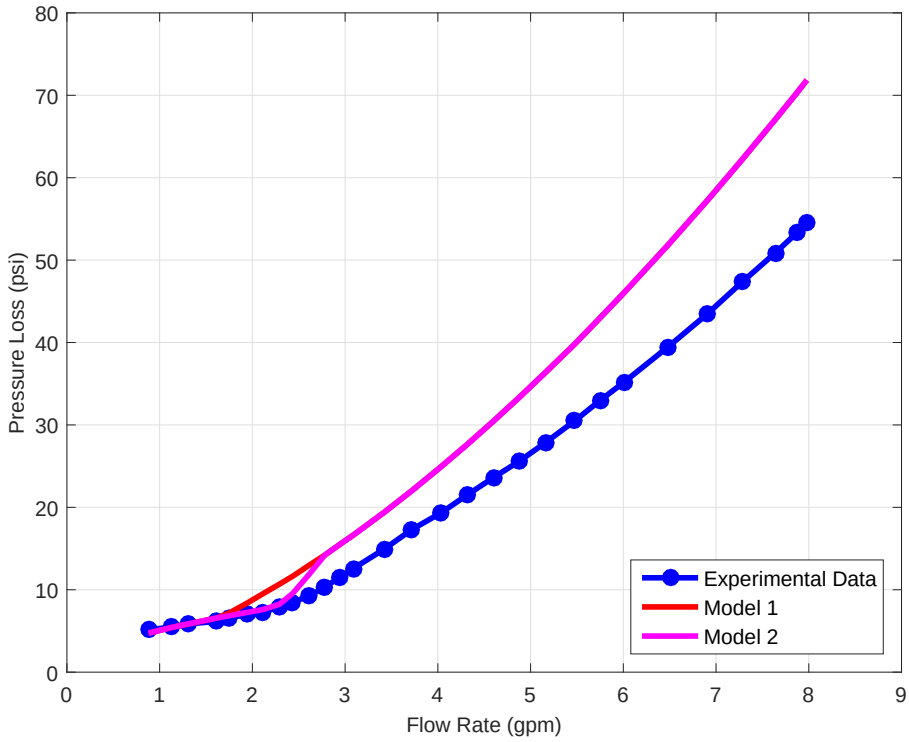

Figure 4.20: Comparison between values obtained from experimental data and the Dodge-Metzner for Mud G.

The pressure loss versus flow rate test showed a pressure loss less than what was expected in the model at the given fluid rheology. Model 1 reaches transition and begins to deviate from the transitional flow at a flow rate of 1.62

gpm and an associated Reynolds number of about 1600. Model 2 transitions from flow rates of 2.4 to 2.7 gpm.

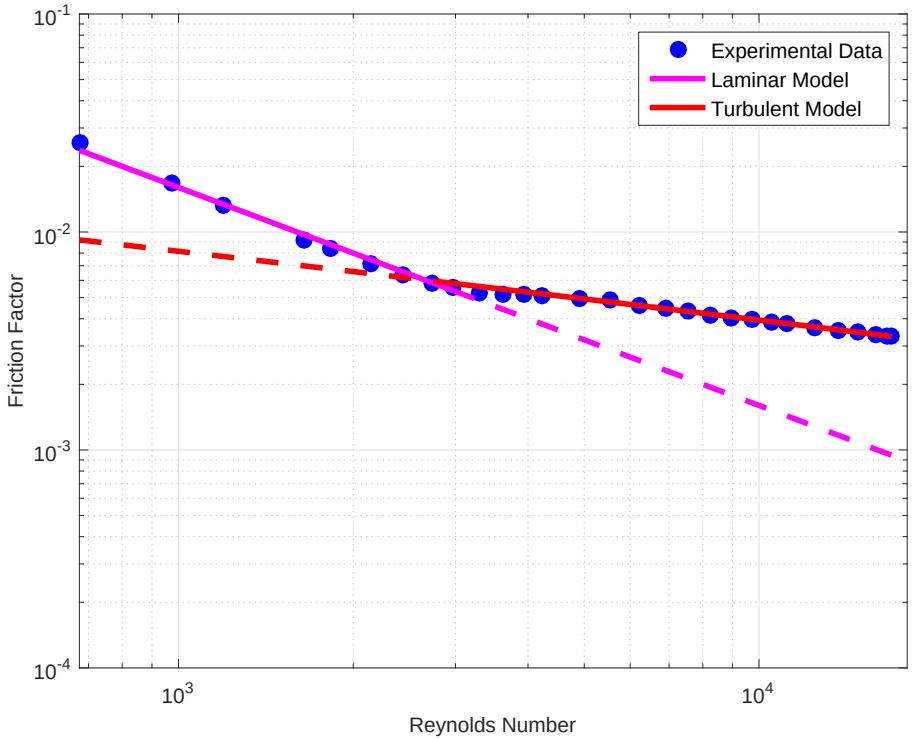

Figure 4.21: Friction factor versus Reynolds number for Mud G.

Figure 4.21 shows that the fluid begins to deviate from the laminar flow profile at a Reynolds number of about 2700. After this point, there is no spike in friction factor, although there is a very slight inflection point at a Reynolds number of about 4200. All points after this Reynolds number were set as turbulent and a curve was fit. Because of the smooth transition from laminar to turbulent flow, a transitional flow fit is not necessary. However, because there is an inflection in the curve after the laminar flow one is included here.

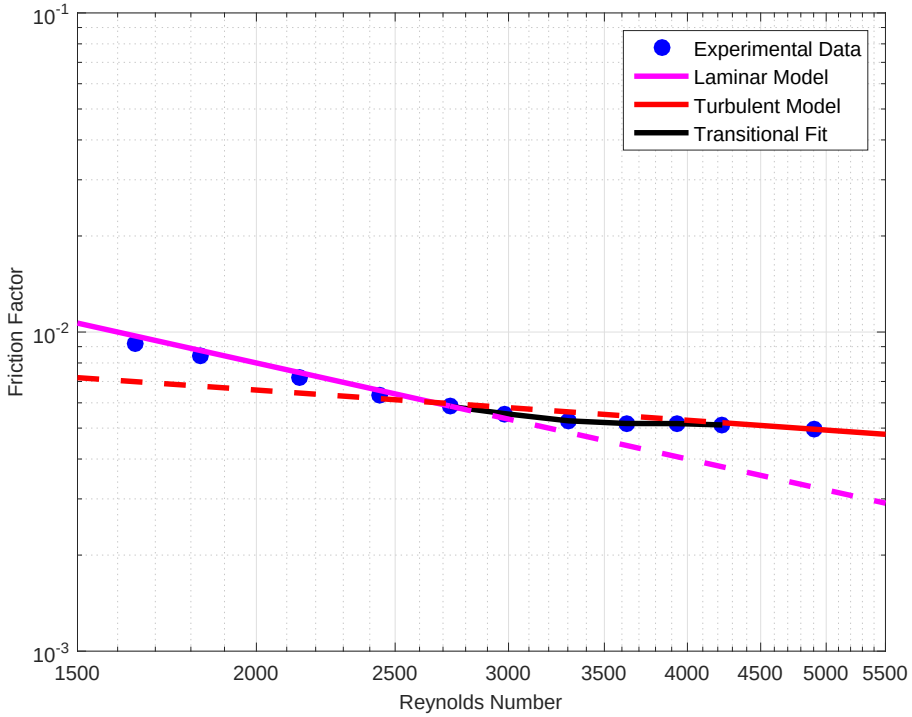

Figure 4.22: Transitional friction factor versus Reynolds number for Mud G.

The transitional fit shown for the given mud is very smooth, similar to the polymer mud. Additionally, the pressure loss is significantly less than what is expected using the Dodge-Metzner formula.

Upon contacting the company, the mud was shown to contain high levels of polymers. This shows that adaptive and flexible models, like the one used in this analysis, are necessary to estimate ECD in real world applications.

4.2.5 Mud H (Synthetic Based Field Mud)

A reconditioned synthetic based field tested mud was tested in a manner similar to the water based field mud. The mud was diluted with a synthetic

base oil. The mud was diluted to a density of 9.9 ppg. The rheology of the given mud was much thicker than the previous rheologies tested for the turbulent tests. Flow rate could only be varied from 1.29 - 6.67 gpm with Reynolds number from about 600 to 3600.

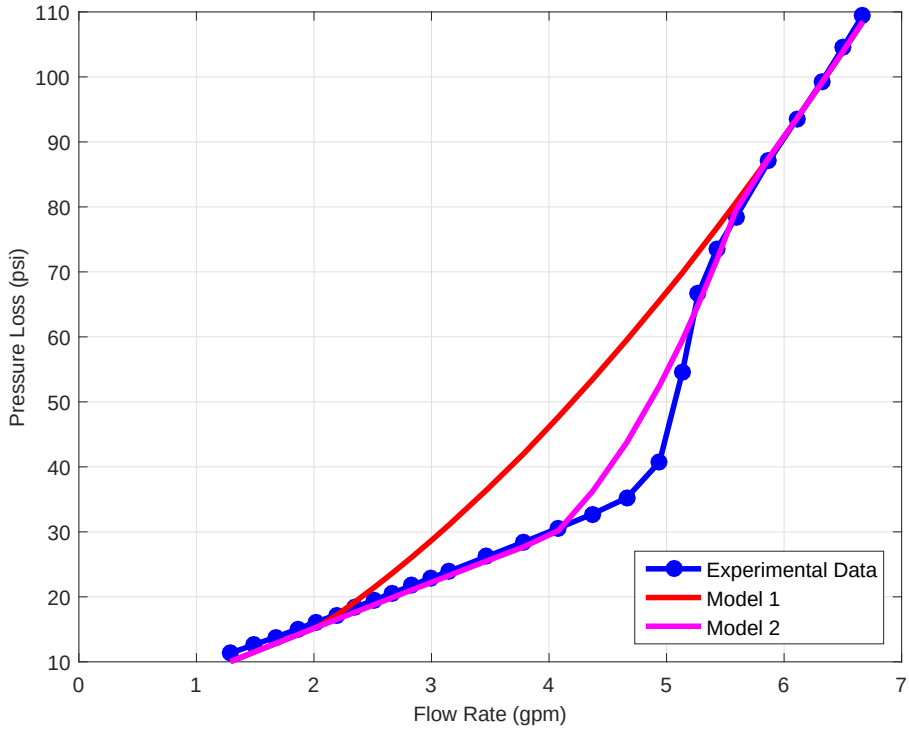

Figure 4.23: Comparison between values obtained from experimental data and the Dodge-Metzner for Mud H.

Figure 4.23 shows pressure loss versus flow rate. Similar to the previous muds with clay, the model shows a good fit to the experimental data at low laminar flow rates and highly turbulent flow rates. Model 1 shows a transition point at about 2 gpm. Model 2 shows a transition region from 4.0 to 5.3 gpm. For this fluid, the transitional region given in Model 2, appears to be more

accurate. However, the estimated friction factor values within this region are shown to be incorrect. Because of this, it has been shown that direct measurement of fluid friction factor is superior to using a model.

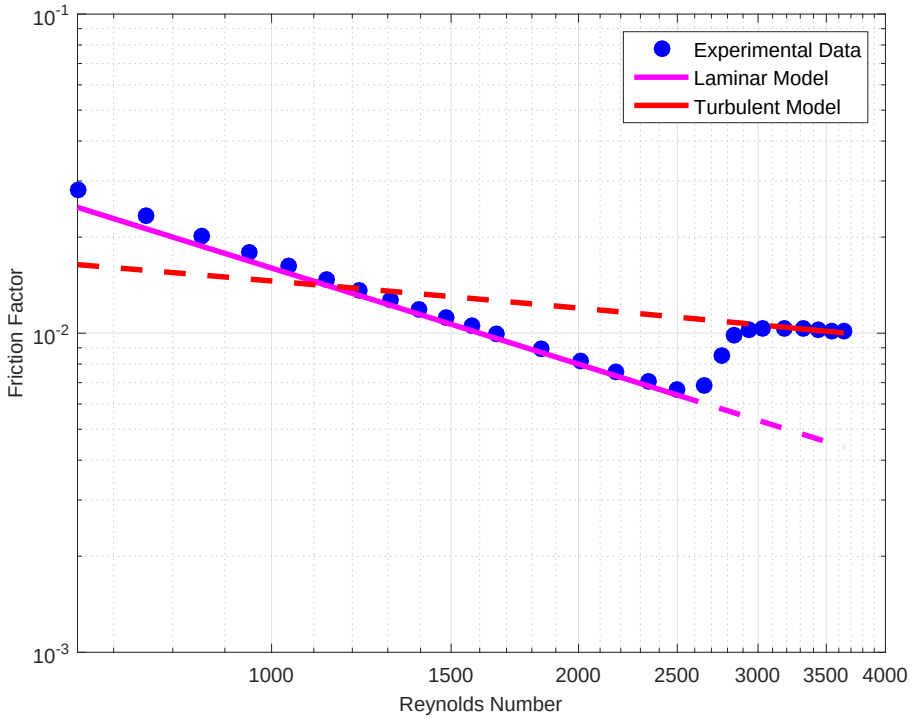

Figure 4.24: Friction factor versus Reynolds number for Mud H.

The fluid follows the laminar friction factor model up to a Reynold number of 2500. The friction factor then increases within the turbulent flow range. At a Reynolds number of 3500 the experimental data has an inflection point and this is set as the start of fully turbulent flow. The transition region ranges from Reynolds number of 2500 to 3500 and is shown in Figure 4.25.

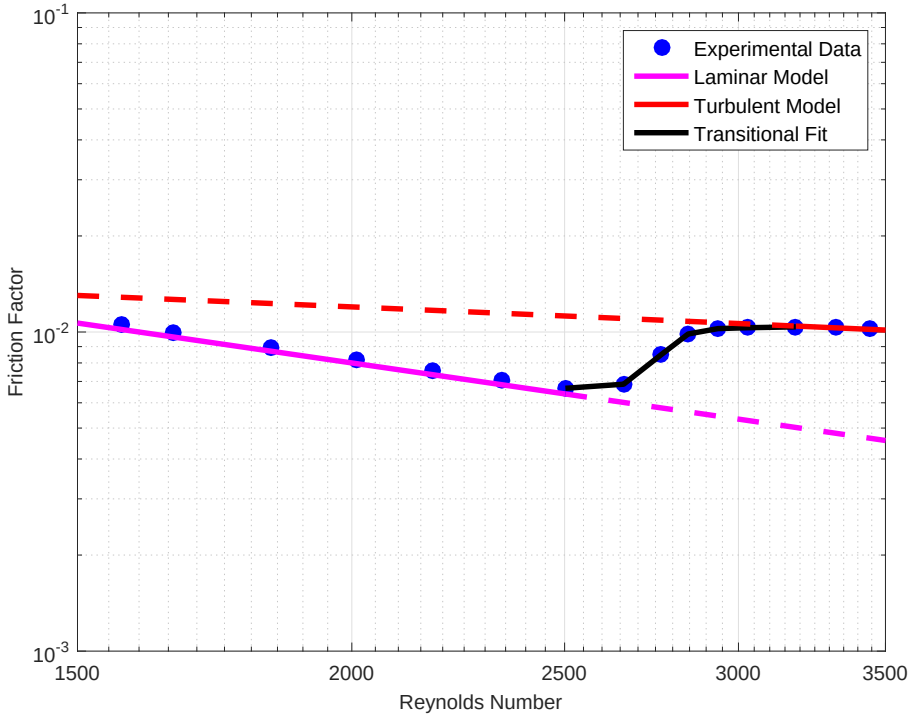

Figure 4.25: Transitional friction factor versus Reynolds number for Mud H.

4.2.6 Overview

Mud Type	A	B	C
Mud D	0.000313	0.07622	-0.2689
Mud E	0.001871	405.0	-1.446
Mud F	0.001598	0.5751	-0.5406
Mud G	-0.00049	0.06417	-0.2902
Mud H	-0.00568	0.07903	-0.1971

Table 4.7: Turbulent flow parameters for each mud tested at turbulent flow.

Mud	Model 1	Model 2	Experimental
Mud A	1270	2510	2340
Mud B	1970	2720	4500
Mud C	2240	2790	2120
Mud D	1290	2440	2290
Mud E	1940	2760	2690
Mud F	1450	2500	2460
Mud G	1710	2630	2440
Mud H	1070	2150	2010

Table 4.8: Critical Reynolds number comparison between the models and the experimental data. Values from rheology test data are also included.

4.3 Friction Reduction Tests

Friction reducers used in the field were tested and compared. Tests were performed in freshwater and 2-times saltwater brine (70 grams of InstantOcean® Sea Salt per liter). In total, 5 products used in the field as friction reducers for frac water were tested.

The effects of fluid concentration for Product 1 and Product 2 were tested in Figures 4.26 and 4.27 respectively. It can be seen that, as expected,

there is a plateau at which increasing friction reducer concentration is no longer beneficial. This is important because the optimal concentration will change based upon the fluid and the friction reducer is being used in. Finding this value during a fracking operation will allow for simple friction reducer optimization.

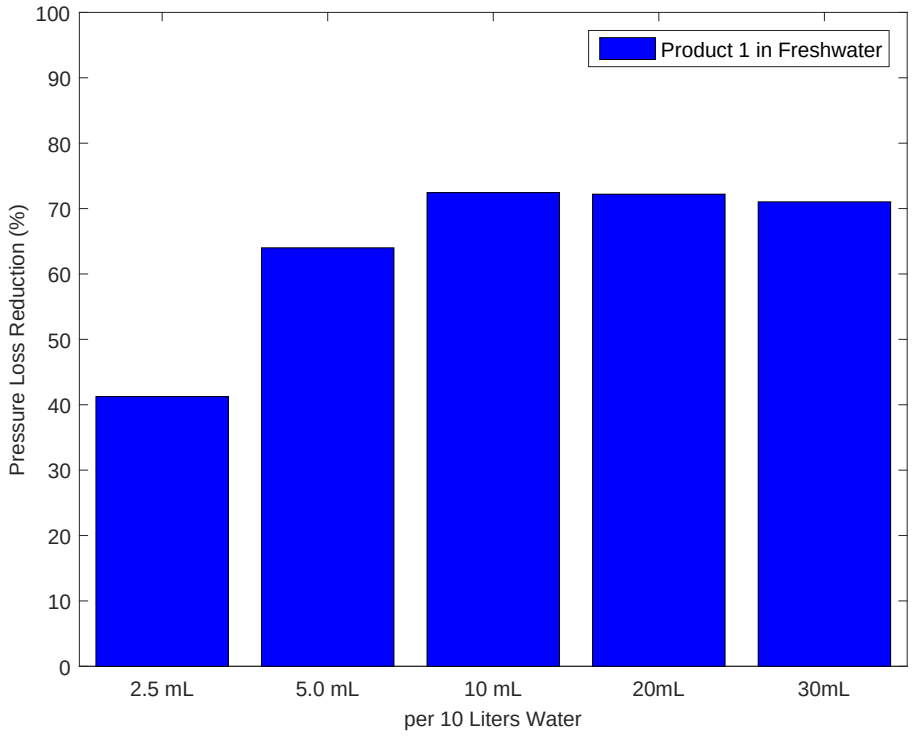

Figure 4.26: Percentage pressure loss reduction based upon concentration for Product 1 in freshwater. Reynold numbers from 80,000 to 100,000.

Figure 4.28 shows the friction reduction of each product at the maximum Reynolds number tested for both freshwater and saltwater. The plot highlights the benefit of using freshwater instead of brine when trying to pump frac water at a high velocity.

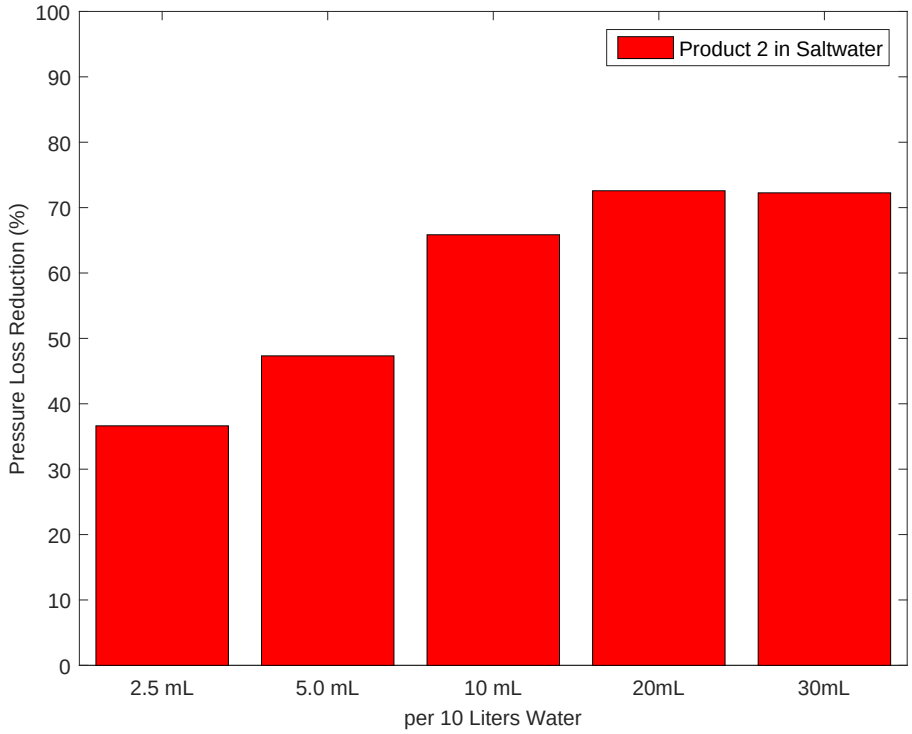

Figure 4.27: Percentage pressure loss reduction based upon concentration for Product 2 in saltwater. Reynold numbers from 80,000 to 100,000.

Because the water used varies based upon location, testing various friction reducers, or the quantity of friction reducer required, could be of extreme benefit when trying to achieve high flow rates. Tests on the product effectiveness and longevity can both help benefit the field.

Figure 4.29 compares the pressure loss reduction of all of the products used in saltwater and freshwater. The data in blue shows the freshwater results while the data in red shows the saltwater results. For all the freshwater tests, the effectiveness of the friction reducer was not very dependent upon the Reynolds number. Additionally, all of the products tested had very

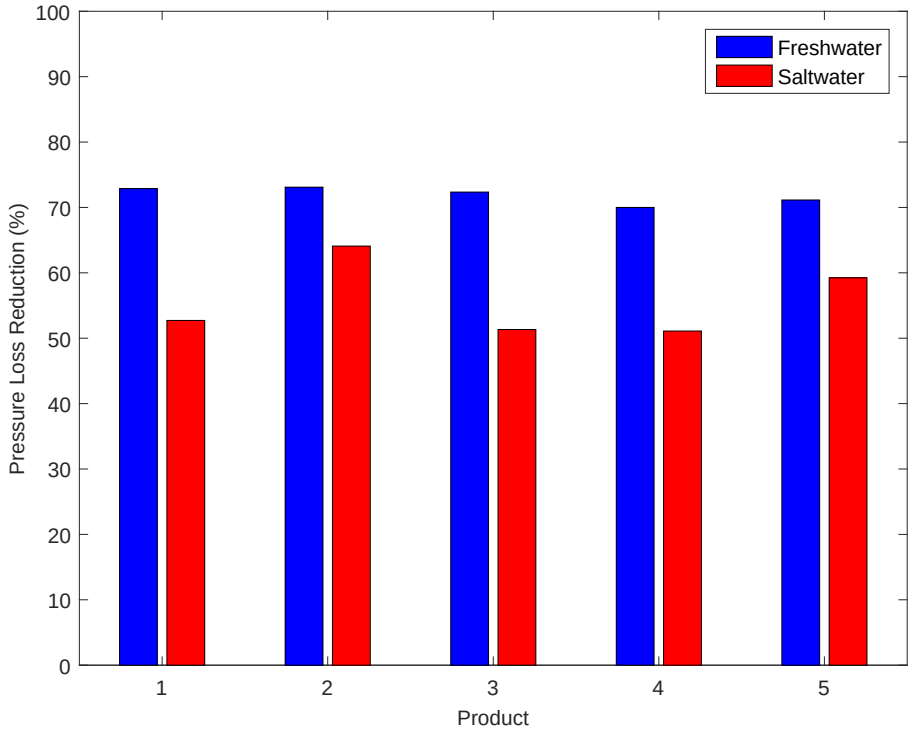

Figure 4.28: Comparison for various products in freshwater and saltwater. Reynolds numbers approximately 100,000.

similar results for freshwater.

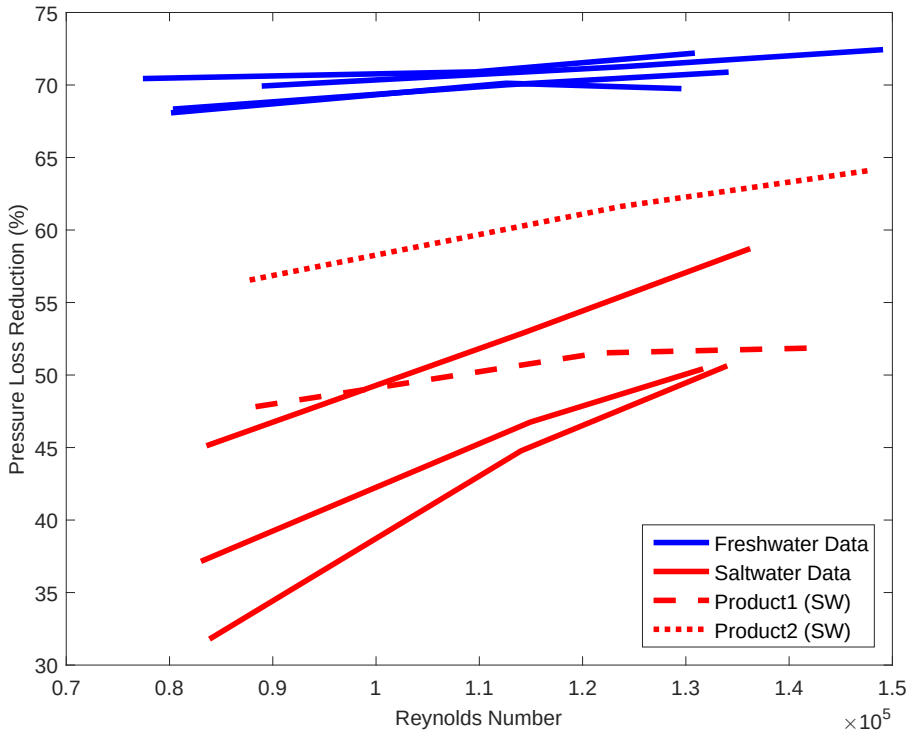

Figure 4.29: Percentage pressure loss reduction vs Reynolds number. Products 1 and 2 were both run in saltwater and compared.

The saltwater results show much more variation depending upon the product and Reynolds number. The results from Product 1 and Product 2 (each at 10 mL per L) are singled out for comparison. Product 2 (designed for saltwater) performs better at all of the Reynolds numbers tested in salt; however, it is 3-times as expensive. The fluid shows a significant cost improvement in saltwater, and a negligible one in the freshwater.

Chapter 5

Conclusions and Future Work

5.1 Conclusions

An alternative approach to the industry standard rotational viscometer for mud rheology characterization has proven effective through the use of a fully automated pipe viscometer. The method relies on flow rate and pressure loss to develop a rheogram, from which essential rheological parameters can be derived using a suitable rheological model (e.g. Bingham Plastic, Power Law, Yield Power Law/Herschel Bulkley, Cassons Model) etc.

In addition to rheology, the pipe viscometer allows for real time calculations of friction factor, critical Reynolds number, and density. These inputs are extremely important when drilling in an extremely tight 'mud window'. The parameters can be directly input into high-fidelity hydraulics models like DGD, MPD, etc.

The hardware and software required for automated drilling fluid characterization via the pipe viscometer has been developed and tested at the University of Texas at Austin. After testing, it is argued that the pipe viscometer yields the same information as traditional rotational viscometers provide, but with important added advantages. A pipe viscometer lends itself very well

to robust automation. This was demonstrated by our lab experiments, which were done with a fully automated set-up that did not require any human interaction for either its operation or its mud rheology characterization using computer data analysis. Muds tested included weighted lab based muds, a water based field mud, and a synthetic based field mud. Applications range from mud characterization in mud mixing plants to advanced deepwater drilling operation in narrow-margin downhole environments.

The system proved very effective in monitoring changes in real time. The changes found by the pipe viscometer were similarly shown in the rotational viscometer. Because the pipe viscometer lends itself well to automation, it is assumed that the pipe viscometer would catch a viscosity change before a 'mud check' the field.

Of major significance is the success of the instrument in measuring fluid pressure loss for transitional and turbulent flows. With this development, semi-empirical based models are no longer required to estimate what the pressure loss will be at a given Reynolds number. Instead, a model can be developed in real time from the fluid behavior in transitional and turbulent flow. Critical Reynolds number (a parameter of importance for cuttings removal) can be directly calculated for the fluid in real time.

Muds made with polymers showed friction reducing properties in turbulent flow. These friction reduction properties can help to reduce ECD in muds.

The setup allows for a real time evaluation of friction factor for frac fluids. It has been noted in this thesis that the effectiveness of many friction reducers is significantly reduced in the presence of salt. Additionally, it was found that the effectiveness of a friction reducer was dependent upon Reynolds number in brines. Finally, the automated pipe viscometer provides a simple means for optimizing friction reducer concentration.

5.2 Future Work

The system is ready to be tested and verified in the field. The rheology and transitional/turbulent pressure loss of the pipe viscometer (tested in real time) can be directly compared to the rheology from the rotational viscometer as well as the modeled pressure loss. The added value of the continuous monitoring, improvements in rig safety and efficiency, and turbulent flow measurements can be fully understood after directly comparing it to the current systems in use.

Understanding transition points for Yield Power Law fluids is actively being researched. A deeper study into critical Reynolds number would be beneficial due to the large pressure increase and cuttings transport improvement associated with this point. More models should be tested with the automated pipe viscometer to find better trends. Models involving polymer based muds should be further explored.

An economic analysis on frac fluids using the pipe viscometer should be performed. Additionally, tests involving the use of friction reducers in drilling

muds should be performed.

Appendices

Appendix A

Rheology Mud Properties

A.1 Mud A (Clay Based Mud)

Component	SG	Mass (g)	Volume (mL)
Water	1.00	329.00	329.00
Bentonite	2.40	24.00	10.00
Barite	4.20	46.20	11.00
Rev Dust	1.20	0.00	0.00
Total	1.14	399.20	350.00

Table A.1: Composition of mud used for clay based mud rheology test (1 g/350 mL = 1 lb/ bbl) mud weight = 9.50 ppg).

RPM	Dial Reading	Shear Rate (1/s)	Shear Stress (Pa)
600	44.8	1021.38	22.89
300	32.5	510.69	16.61
200	28.0	340.46	14.32
100	22.9	170.23	11.68
60	20.0	102.14	10.20
30	18.7	51.07	9.53
6	17.2	10.21	8.76
3	17.1	5.11	8.71

Table A.2: Rheology measurements recorded via OFITE Model 900 Viscometer for clay based mud rheology test.

Flow Rate (gpm)	**Pressure Loss Large Pipe (psi)**
0.89	2.93
1.04	3.08
1.19	3.10
1.37	3.24
1.53	3.43
1.70	3.61
1.86	3.79
2.04	3.99
2.21	4.19
2.38	4.41
2.55	4.61
2.90	4.97
3.20	5.25
3.51	5.67
3.81	6.24
4.38	7.19
4.81	8.16
5.18	10.74
5.52	12.19
5.81	13.37
6.08	14.39
6.31	15.32
6.53	16.22
6.74	17.10
6.94	17.94
7.13	18.75

Table A.3: Flow rate and pressure loss measurements for clay based mud rheology test (Pipe ID = 0.43 in, Length = 10 ft).

A.2 Mud A* (Clay Based Mud Influx)

Component	SG	Mass	Volume
Water	1.00	315.84	315.84
Bentonite	2.40	27.84	11.60
Barite	4.20	44.35	10.56
Rev Dust	1.20	14.40	12.00
Total	1.20	419.20	350.00

Table A.4: Composition of mud used for clay based mud influx test, mud weight = 10.00 ppg).

RPM	Dial Reading	Shear Rate	Shear Stress
600	73.8	1021.38	37.68
300	55.8	510.69	28.49
200	48.9	340.46	24.99
100	40.2	170.23	20.54
60	38.1	102.14	19.44
30	34.0	51.07	17.38
6	30.8	10.21	15.70
3	30.2	5.11	15.42

Table A.5: Rheology measurements recorded via OFITE Model 900 Viscometer for clay influx rheology test.

Flow Rate (gpm)	**Pressure Loss Large Pipe (psi)**
0.84	5.563
1.01	5.405
1.18	5.686
1.35	5.957
1.51	6.220
1.67	6.470
1.84	6.753
2.00	6.980
2.16	7.254
2.32	7.369
2.48	7.604
2.79	8.030
3.11	8.437
3.41	8.827
3.73	9.254
4.29	10.091
4.73	10.977
5.11	11.684
5.48	12.679
5.81	13.827
6.06	14.577
6.27	15.012
6.47	15.435
6.66	15.919
6.86	16.353

Table A.6: Flow rate and pressure loss measurements for clay influx rheology test (Pipe ID = 0.43 in, Length = 10 ft).

A.3 Mud B (Polymer Based Mud)

Component	SG	Mass	Volume
Water	1.00	337.00	337.00
Pac R	1.20	2.20	1.83
Barite	4.20	46.90	11.17
Total	1.10	386.10	350.00

Table A.7: Composition of mud used for polymer based mud rheology test (1 g/350 mL = 1 lb/ bbl, mud weight = 9.16 ppg).

RPM	Dial Reading	Shear Rate	Shear Stress
600	88.0	1021.38	44.96
300	66.7	510.69	34.04
200	55.6	340.46	28.39
100	40.1	170.23	20.49
60	30.8	102.14	15.70
30	19.9	51.07	10.15
6	6.9	10.21	3.54
3	3.7	5.11	1.87

Table A.8: Rheology measurements recorded via OFITE Model 900 Viscometer for polymer based mud rheology test.

Flow Rate (gpm)	Pressure Loss Large Pipe (psi)
0.94	5.646
1.12	6.256
1.29	6.665
1.46	7.070
1.63	7.412
1.79	7.724
1.94	7.981
2.09	8.238
2.25	8.478
2.42	8.724
2.60	8.965
2.77	9.174
2.93	9.192
3.09	9.448
3.41	9.709
3.73	10.103
4.05	10.450
4.36	10.768
4.67	11.088
4.97	11.354
5.53	11.597
6.08	12.090
6.84	12.438
7.56	13.049
8.24	13.586
8.88	14.258
9.47	14.764
9.99	15.242
10.51	15.701
10.91	16.180

Table A.9: Flow rate and pressure loss measurements for polymer based mud rheology test (Pipe ID = 0.43 in, Length = 10 ft).

A.4 Mud C (Synthetic Based Field Mud)

RPM	Dial Reading	Shear Rate	Shear Stress
600	91.4	1021.38	46.68
300	52.7	510.69	26.91
200	38.3	340.46	19.58
100	22.2	170.23	11.35
60	15.9	102.14	8.14
30	10.7	51.07	5.46
6	5.0	10.21	2.54
3	4.6	5.11	2.35

Table A.10: Rheology measurements recorded via OFITE Model 900 Viscometer for synthetic based field mud rheology test. Mud Weight = 10.00 ppg.

Flow Rate (gpm)	**Pressure Loss Large Pipe (psi)**
0.80	6.891
0.95	7.939
1.11	8.939
1.26	9.870
1.42	10.936
1.59	11.874
1.76	12.821
1.93	13.751
2.10	14.680
2.27	15.616
2.43	16.502
2.74	18.340
3.04	20.035
3.32	21.602
3.59	23.126
4.07	25.852
4.51	28.141
4.88	29.990
5.17	31.217
5.44	32.513
5.67	35.748
5.78	41.860
5.84	49.094
5.96	53.866

Table A.11: Flow rate and pressure loss measurements for synthetic based field mud rheology test (Pipe ID = 0.43 in, Length = 10 ft).

Appendix B

Transitional/Turbulent Mud Properties

B.1 Mud D (Clay Based Mud)

Component	SG	Mass	Volume
Water	1.00	322.14	322.14
Bentonite	2.40	22.00	9.17
Barite	4.20	43.52	10.36
RevDust	1.20	10.00	8.33
Total	1.14	397.66	350.00

Table B.1: Composition of mud used for clay based mud transitional/turbulent test (1 g/350 mL = 1 lb/ bbl mud weight = 9.50 ppg).

RPM	DR	Shear Rate	Shear Stress
600	45.6	1021.38	23.29
300	30.2	510.69	15.42
200	23.6	340.46	12.05
100	16.4	170.23	8.38
60	12.8	102.14	6.54
30	11.0	51.07	5.62

Table B.2: Rheology measurements recorded via OFITE Model 900 Viscometer for clay transitional/turbulent test.

Flow Rate (gpm)	Pressure Loss (psi)
0.92	4.635
1.15	5.985
1.34	7.353
1.53	8.171
1.70	8.500
1.89	9.003
2.07	9.545
2.23	10.106
2.39	11.319
2.56	13.078
2.72	16.430
2.88	18.475
3.04	20.531
3.20	22.345
3.51	26.660
3.83	30.970
4.13	35.112
4.42	39.332
4.72	43.930
4.98	48.182
5.22	52.265
5.44	55.959
5.66	59.716
5.86	63.226
6.24	70.241
6.57	76.771
6.87	82.586
7.14	87.812
7.39	92.890

Table B.3: Flow rate and pressure loss measurements for clay based mud transitional/turbulent test (Pipe ID = 0.305 in, Length = 10 ft).

B.2 Mud E (Polymer Based Mud)

Component	SG	Mass	Volume
Water	1.00	328.61	328.61
Pac-R	1.50	0.50	0.33
NewZan	1.50	1.00	0.67
Barite	4.20	50.65	12.06
RevDust	1.20	10.00	8.33
Total	1.12	390.76	350.00

Table B.4: Composition of mud used for polymer based mud transitional/turbulent test (1 g/350 mL = 1 lb/ bbl mud weight = 9.33 ppg).

RPM	DR	Shear Rate	Shear Stress
600	34.6	1021.38	17.67
300	26.1	510.69	13.33
200	22.4	340.46	11.44
100	18.2	170.23	9.29
60	14.1	102.14	7.20
30	12.1	51.07	6.18

Table B.5: Rheology measurements recorded via OFITE Model 900 Viscometer for polymer transitional/turbulent test.

Flow Rate (gpm)	**Pressure Loss (psi)**
0.93	4.270
1.28	5.320
1.63	6.037
1.99	6.734
2.33	7.393
2.67	8.201
3.01	8.968
3.33	9.822
3.83	11.217
4.48	13.205
5.13	15.421
5.76	18.444
6.38	21.735
7.27	26.897
8.14	32.576
8.91	38.002
9.58	43.287
10.20	48.423
10.75	52.969

Table B.6: Flow rate and pressure loss measurements for polymer based mud transitional/turbulent test (Pipe ID = 0.305 in, Length = 10 ft).

B.3 Mud F (Clay and Polymer Based Mud)

Component	SG	Mass	Volume
Water	1.00	326.22	326.22
Pac-LV	1.50	0.90	0.60
Bentonite	2.40	12.00	5.00
Barite	4.20	41.35	9.85
RevDust	1.20	10.00	8.33
Total	1.09	390.47	350.00

Table B.7: Composition of mud used for clay and polymer based mud transitional/turbulent test (1 g/350 mL = 1 lb/ bbl mud weight = 9.08 ppg).

RPM	DR	Shear Rate	Shear Stress
600	35.7	1021.38	18.23
300	23.5	510.69	12.00
200	18.1	340.46	9.24
100	11.1	170.23	5.67
60	7.1	102.14	3.63
30	5.0	51.07	2.55

Table B.8: Rheology measurements recorded via OFITE Model 900 Viscometer for clay and polymer transitional/turbulent test.

Flow Rate (gpm)	Pressure Loss (psi)
0.89	5.261
1.15	5.787
1.37	6.340
1.56	6.853
1.73	7.473
1.90	8.072
2.07	8.750
2.24	9.316
2.40	10.020
2.56	11.500
2.72	15.429
2.88	17.061
3.04	18.680
3.19	20.347
3.51	23.769
3.83	26.729
4.15	29.942
4.46	32.889
4.75	36.089
5.05	39.701
5.34	43.151
5.61	46.286
5.87	49.457
6.11	52.353
6.55	58.114
6.96	63.443
7.36	68.616
7.72	73.592
8.04	78.225
8.33	82.437

Table B.9: Flow rate and pressure loss measurements for clay and polymer based mud transitional/turbulent test (Pipe ID = 0.305 in, Length = 10 ft).

B.4 Mud G (Water Based Field Mud)

RPM	DR	Shear Rate	Shear Stress
600	32.7	1021.38	16.70
300	23.7	510.69	12.10
200	19.0	340.46	9.70
100	12.8	170.23	6.54
60	8.9	102.14	4.55
30	6.1	51.069	3.12

Table B.10: Rheology measurements recorded via OFITE Model 900 Viscometer for water based field mud transitional/turbulent test.

Flow Rate (gpm)	Pressure Loss (psi)
0.88	5.151
1.13	5.452
1.30	5.845
1.62	6.171
1.74	6.578
1.94	6.997
2.12	7.301
2.29	7.906
2.43	8.486
2.61	9.233
2.78	10.312
2.94	11.485
3.09	12.589
3.42	14.933
3.72	17.317
4.03	19.301
4.32	21.533
4.60	23.615
4.88	25.612
5.16	27.854
5.47	30.487
5.75	32.974
6.01	35.209
6.48	39.449
6.90	43.415
7.28	47.323
7.64	50.892
7.87	53.316
7.98	54.468

Table B.11: Flow rate and pressure loss measurements for water based field mud transitional/turbulent test (Pipe ID = 0.305 in, Length = 10 ft).

B.5 Mud H (Synthetic Based Field Mud)

RPM	DR	Shear Rate	Shear Stress
600	50.5	1021.38	25.79
300	26.4	510.69	13.48
200	18.6	340.46	9.50
100	11.5	170.23	5.87
60	6.9	102.14	3.52
30	4.3	51.069	2.20

Table B.12: Rheology measurements recorded via OFITE Model 900 Viscometer for synthetic based mud transitional/turbulent test.

Flow Rate (gpm)	Pressure Loss (psi)
1.29	11.342
1.49	12.629
1.68	13.827
1.86	15.031
2.02	16.129
2.19	17.229
2.35	18.386
2.51	19.474
2.67	20.585
2.83	21.721
2.99	22.875
3.15	23.920
3.47	26.189
3.78	28.420
4.08	30.574
4.37	32.753
4.66	35.211
4.94	40.757
5.13	54.507
5.27	66.642
5.43	73.544
5.59	78.431
5.87	87.023
6.11	93.588
6.32	99.276
6.50	104.493
6.67	109.524

Table B.13: Flow rate and pressure loss measurements for synthetic based field mud transitional/turbulent test (Pipe ID = 0.305 in, Length = 10 ft).

Appendix C

Derivation of Viscometric Pipe Flow Equations

This derivation is based off of the works provided in Karimi Varejah et al. (2015)

The flow rate through the short pipe segment with diameter D and length ΔL is provided as:

$$Q = 2\pi \int_0^R v(r) r dr \tag{C.1}$$

We assume a no slip boundary condition meaning that:

$$v(R) = 0 \tag{C.2}$$

Integrating by parts, we obtain:

$$Q = -\pi \int_0^R r^2 \frac{dv}{dr} dr \tag{C.3}$$

The velocity gradient (shear rate) is a function of the shear stress. Assuming isothermal, steady state flow of fluid with constant density gives the momentum balance as:

$$\tau = \frac{r}{2}\frac{dp}{dl} \tag{C.4}$$

Hence, the shear rate at the wall is:

$$\tau_w = \frac{R}{2}\frac{dp}{dl} \tag{C.5}$$

By dividing Equation C.4 by Equation C.5 we obtain:

$$\frac{\tau(r)}{\tau_w} = \frac{r}{R} \tag{C.6}$$

We then multiply Equation C.6 by R to obtain:

$$r = R\frac{\tau(r)}{\tau_w} \tag{C.7}$$

Plugging in Equation C.7 to Equation C.3 gives:

$$Q = -\pi \int_0^{\tau_w} \left(\frac{R}{\tau_w}\right)^3 \frac{dv}{dr}\tau^2 d\tau \tag{C.8}$$

We know that shear rate is a function of shear stress:

$$f(\tau) = \frac{dv}{dr} \tag{C.9}$$

Using Leibniz's formula for differential integrals, Equation C.8 can be rearranged to:

$$\frac{d(Q\tau_w^3)}{d\tau_w} = -\pi R^3 f(\tau_w)\tau_w^2 \tag{C.10}$$

Therefore, the shear rate at the wall can be obtained from:

$$f(\tau_w) = \left(\frac{dv}{dr}\right)_R = \dot{\gamma}_w = \frac{1}{\pi R^3 \tau_w^2}\frac{d(Q\tau_w^3)}{d\tau_w} \tag{C.11}$$

or:

$$\dot{\gamma}_w = \frac{1}{\pi R^3}\tau_w \frac{dQ}{d\tau_w} + \frac{3Q}{\pi R^3} \tag{C.12}$$

We know that:

$$\frac{Q}{\pi R^3} = \frac{v}{R} = \frac{2v}{D} \tag{C.13}$$

and thus:

$$\dot{\gamma}_w = \frac{\tau_w}{4}\frac{d\left(\frac{8v}{D}\right)}{d\tau_w} + \frac{3}{4}\left(\frac{8v}{D}\right) \tag{C.14}$$

The following then holds:

$$\tau_w \frac{d(ln\tau_w)}{d\tau_w} = \left(\frac{8v}{D}\right)\frac{d\left(ln\frac{8v}{D}\right)}{d\left(\frac{8v}{D}\right)} \tag{C.15}$$

Therefore:

$$\frac{d\left(\frac{8v}{D}\right)}{d\tau_w} = \frac{\left(\frac{8v}{D}\right)}{\tau_w} \frac{d\left(ln\frac{8v}{D}\right)}{d\left(ln\tau_w\right)} \tag{C.16}$$

By substituting Equation C.16 into Equation C.14, we obtain the shear rate at the wall:

$$\dot{\gamma}_w = \frac{1}{4}\left[3 + \frac{d\left(ln\frac{8v}{D}\right)}{d\left(ln\tau_w\right)}\right]\left(\frac{8v}{D}\right) \tag{C.17}$$

Introducing the generalized flow behavior index expressed as:

$$N = \frac{d\left(ln\tau_w\right)}{d\left(ln\frac{8v}{D}\right)} \tag{C.18}$$

We get the following:

$$\dot{\gamma}_w = \left(\frac{3N+1}{4N}\right)\left(\frac{8v}{D}\right) \tag{C.19}$$

Bibliography

[1] R. Ahmed and S. Miska. Advanced wellbore hydraulics. In *Advanced Drilling and Well Technology*, pages 191–219. USA Society of Petroleum Engineers, 2009.

[2] H. Blasius. Das ähnlichkeitsgesetz bei reibungsvorgängen in flüssigkeiten. In *Mitteilungen über Forschungsarbeiten auf dem Gebiete des Ingenieurwesens*, pages 1–41. Springer, 1913.

[3] S. Broussard, P. Gonzalez, R. J. Murphy, C. Marvel, et al. Making real time fluid decisions with real time fluid data at the rig site: Results of automated drilling fluid measurement field trials. In *Abu Dhabi International Petroleum Exhibition and Conference*. Society of Petroleum Engineers, 2010.

[4] R. P. Chhabra and J. F. Richardson. *Non-Newtonian flow and applied rheology: engineering applications*. Butterworth-Heinemann, 2011.

[5] R. A. Chilton and R. Stainsby. Pressure loss equations for laminar and turbulent non-newtonian pipe flow. *Journal of Hydraulic Engineering*, 124(5):522–529, 5 1998.

[6] C. F. Colebrook, T. Blench, H. Chatley, E. H. Essex, J. R. Finniecome, G. Lacey, J. Williamson, and G. G. Macdonald. Correspondence. turbu-

lent flow in pipes, with particular reference to the transition region beteen smooth and rough pipe laws. (includes plates). *Journal of the Institution of Civil engineers*, 12(8):393–422, 1939.

[7] M. Collins and W. R. Schowalter. Behavior of non-newtonian fluids in the entry region of a pipe. *AIChE journal*, 9(6):804–809, 1963.

[8] D. W. Dodge and A. B. Metzner. Turbulent flow of non-newtonian systems. *AIChE Journal*, 5(2):189–204, 1959.

[9] O. Erge, A. Karimi, E. M. Ozbayoglu, E. van Oort, et al. Improved ecd prediction and management in horizontal and extended reach wells with eccentric drillstrings. In *IADC/SPE Drilling Conference and Exhibition*. Society of Petroleum Engineers, 2016.

[10] O. Erge, E. M. Ozbayoglu, S. Miska, M. Yu, N. Takach, A. Saasen, R. May, et al. The effects of drillstring-eccentricity,-rotation, and-buckling configurations on annular frictional pressure losses while circulating yield-power-law fluids. *SPE Drilling & Completion*, 2015.

[11] O. Erge, A. Karimi Vajargah, E. M. Ozbayoglun, and E. van Oort. Frictional pressure loss of drilling fluids in a fully eccentric annulus. *Journal of Natural Gas Science and Engineering*, 26:1119–1129, 2015.

[12] M. D. Graham. Drag reduction in turbulent flow of polymer solutions. *Rheology Reviews*, 2(2):143–170, 2004.

[13] G. R. Gray, H. Darley, and W. F. Rogers. *Composition and properties of oil well drilling fluids*. Gulf Publishing Company, Book Division, 1980.

[14] G. L. Hensley, J. Van Dokkum, A. Groeneweg, and G. Stolk. Apparatus and method for real-time measurement of drilling fluid properties, 1985. US Patent 4,557,142.

[15] G. Kalayci, E. M. Ozbayoglu, S Z. Miska, M. Yu, N. Takach, A. Saasen, and R. May. Transition criteria for laminar to turbulent flow for yield power law (ypl) fluids based on stability analysis. In *ASME 2013 Fluids Engineering Division Summer Meeting*. American Society of Mechanical Engineers, 2013.

[16] V. C. Kelessidis, P. Dalamarinis, and Maglione R. Experimental study and predictions of pressure losses of fluids modeled as herschel–bulkley in concentric and eccentric annuli in laminar, transitional and turbulent flows. *Journal of Petroleum Science and Engineering*, 77(3):305–312, 2011.

[17] R. F. Mitchell, S. Miska, et al. *Fundamentals of drilling engineering*. Society of Petroleum Engineers,, 2011.

[18] A. Pilehvari, R. Serth, et al. Generalized hydraulic calculation method for axial flow of non-newtonian fluids in eccentric annuli. *SPE drilling & completion*, 24(04):553–563, 2009.

[19] A. Saasen, T. H. Omland, S. Ekrene, J. Brévière, E. Villard, N. Kaageson-Loes, A. Tehrani, J. Cameron, M. A. Freeman, F. Growcock, et al. Automatic measurement of drilling fluid and drill-cuttings properties. *SPE drilling & completion*, 24(04):611–625, 2009.

[20] P. T. Slatter, F. W. Petersen, and L. Moodie. Rheological characterisation of mineral slurries using balanced beam tube viscometry. *South African Institute of Mining and Metallurgy*, 98:165–170, 1998.

[21] API Specifications. 13a 1993. specification for drilling fluid materials. *American Petroleum Institute*.

[22] API Specifications. 13b-1 2003. recommended practice standard procedure for field testing water-based drilling fluids. *American Petroleum Institute*.

[23] API Specifications. 13b-2 2003. recommended practice standard procedure for field testing oil-based drilling fluids. *American Petroleum Institute*.

[24] T. Stock, E. Ronaes, T. H. Fossdal, J. BjerkasS, et al. The development and successful application of an automated real-time drilling fluids measurement system. In *SPE Intelligent Energy International*. Society of Petroleum Engineers, 2012.

[25] R. Subramanianand, J. J. Azar, et al. Experimental study on friction pressure drop for nonnewtonian drilling fluids in pipe and annular flow.

In *International Oil and Gas Conference and Exhibition in China*. Society of Petroleum Engineers, 2000.

[26] K. Suzuki. Theory and applications of a new viscometer based on annulus liquid flow. In *Developments in Food Engineering*, pages 921–923. Springer, 1994.

[27] B. A. Toms and K. J. Mysels. Proc. first intern. congr. on rheology, 1948.

[28] A. Karimi Vajargah, G. Sullivan, and E. van Oort. Automated fluid rheology and ecd management. In *SPE Deepwater and Drilling Conference*. Society of Petroleum Engineers, 2016.

[29] A. Karimi Vajargah and E. van Oort. Automated drilling fluid rheology characterization with downhole pressure sensor data. In *SPE/IADC Drilling Conference and Exhibition*. Society of Petroleum Engineers, 2015a.

[30] A. Karimi Vajargah and E. van Oort. Determination of drilling fluid rheology under downhole conditions by using real-time distributed pressure data. *Journal of Natural Gas Science and Engineering*, 24:400–411, 2015b.